LA--9080-SR

DE82 010023

LA-9080-SR
Status Report

UC-66b
Issued: November 1981

Hot Dry Rock Geothermal Reservoir Testing: 1978 to 1980

Edited by

Z. V. Dash
H. D. Murphy
G. M. Cremer

Contributors

R. L. Aamodt
R. G. Aguilar
D. W. Brown
D. A. Counce
H. N. Fisher
C. O. Grigsby
H. Keppler*
A. W. Laughlin
R. M. Potter
J. W. Tester
P. E. Trujillo, Jr.
G. Zyvoloski

*Alien Guest Scientist. Federal Institute for Geosciences and National Resources (B.G.R.), Hanover, FEDERAL REPUBLIC OF GERMANY.

Los Alamos National Laboratory
Los Alamos, New Mexico 87545

DISCLAIMER

HOT DRY ROCK GEOTHERMAL RESERVOIR TESTING: 1978 TO 1980

Edited by

Z. V. Dash, H. D. Murphy, and G. M. Cremer

Contributors

R. L. Aamodt, R. G. Aguilar, D. W. Brown, D. A. Counce, H. N. Fisher, C. O. Grigsby, H. Keppler, A. W. Laughlin, R. M. Potter, J. W. Tester, P. E. Trujillo, Jr., and G. Zyvoloski

ABSTRACT

Experimental results and re-evaluation of the Phase I Hot Dry Rock Geothermal Energy reservoirs at the Fenton Hill field site are summarized. This report traces reservoir growth as demonstrated during Run Segments 2 through 5 (January 1978 to December 1980). Reservoir growth was caused not only by pressurization and hydraulic fracturing, but also by heat extraction and thermal contraction effects. Reservoir heat-transfer area grew from 8000 to 50 000 m^2 and reservoir fracture volume grew from 11 to 266 m^3. Despite this reservoir growth, the water loss rate increased only 30%, under similar pressure environments. For comparable temperature and pressure conditions, the flow impedance (a measure of the resistance to circulation of water through the reservoir) remained essentially unchanged, and if reproduced in the Phase II reservoir under development, could result in "self pumping." Geochemical and seismic hazards have been nonexistent in the Phase I reservoirs. The produced water is relatively low in total dissolved solids and shows little tendency for corrosion or scaling. The largest microearthquake associated with heat extraction measures less than -1 on the extrapolated Richter scale.

I. INTRODUCTION

The basic idea in extracting energy from hot dry rock (HDR) is to form a manmade geothermal reservoir by drilling into high-temperature, low-permeability basement rock and hydraulically fracturing the rock. A circulation loop is then formed by drilling a second hole and forcing water to sweep heat

from the rock surface in the fractured region between the wellbores. The hot water produced at the surface is used for generating electricity or space heating.

The HDR reservoirs at Fenton Hill are located in the Jemez Mountains of northern New Mexico as shown in Fig. 1. Although the focus of this report is upon the Phase I reservoir (essentially a research system that uses wells EE-1 and GT-2) occasional reference will be made to the Phase II or engineering reservoir. The two wells for the Phase II reservoir, EE-2 and EE-3, were completed in August 1981.

The first deep borehole of the Phase I reservoir, Geothermal Test-2 (GT-2) was drilled in granitic rock to a depth of 2.929 km (9610 ft) where the temperature was 197°C (386°F). A series of hydraulic fracturing experiments was performed in GT-2. Energy Extraction-1 (EE-1) borehole was drilled toward the largest of the GT-2 fractures in an effort to complete the heat-extraction

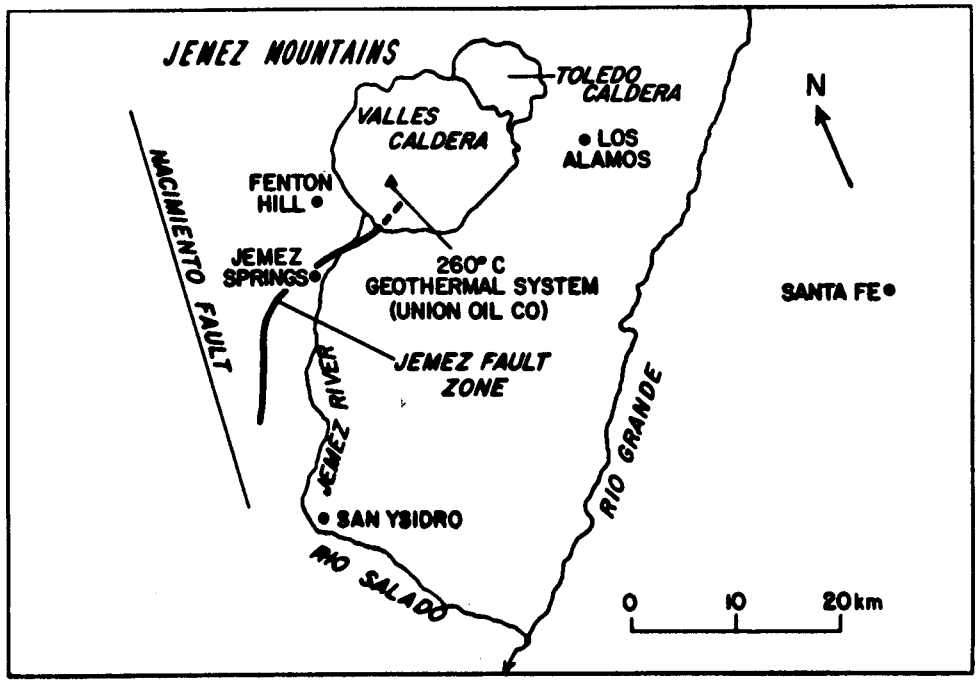

Fig. 1.
Location of Fenton Hill Hot Dry Rock site in the Jemez Mountains of northern New Mexico.

system. The intent was to produce a large vertical spacing between the inlet and outlet locations in order to maximize the effective heat-transfer area while still achieving reasonably low flow impedance. Low flow impedance is required for high rates of heat extraction as the working pressure drop is limited by tectonic stress considerations; excessive pressures normally result in greater downhole water losses. After trying several methods of improving the communication between the boreholes, an acceptable connection was achieved by sidetracking GT-2 at 2.5 km and redrilling it towards the top of a large fracture centered at about 2.75 km in EE-1. Several paths were drilled and eventually one, which penetrated several major natural joints or natural fractures, but probably did not intersect the major fracture, was obtained. This path had low enough flow resistance to proceed with a heat-extraction test. The combination of the original GT-2 wellbore and the redrilled path is referred to as the GT-2B wellbore. In subsequent testing of the reservoir, EE-1 was used as the injection well and GT-2B was used as the production or extraction well.

Reservoir performance was first evaluated by a 75-day period of closed-loop operation from January 28 to April 13, 1978. The assessment of this first reservoir in EE-1 and GT-2B is referred to as "Run Segment 2," or the "75-day test." (Run Segment 1 consisted of a 4-day precursor experiment conducted in September 1977.) Hot water from GT-2B was directed to a water-to-air heat exchanger where the water was cooled to 25°C before reinjection. Makeup water, required to replace downhole losses to the rock surrounding the fracture, was added to the cooled water and pumped down EE-1, and then through the fracture system. Heat was transferred to the circulating water by thermal conduction through the nearly impervious rock adjacent to the fracture surfaces. The average thermal power extracted during Run Segment 2 was 3.1 MWt, evaluated at the surface. The flow impedance, a measure of the pressure loss through the reservoir per unit flow rate, initially 1.7 GPa s/m^3 (16 psi/gpm), decreased by a factor of five as thermal contraction and continued pressurization resulted in the opening of natural joints that provided additional communication with the producing well. Water losses to the rock surrounding the fracture steadily diminished, and eventually this loss rate was about 1% of the injected rate. The geochemistry of the produced fluid was benign, and the seismic effects associated with heat extraction were immeasurably small. However, the relatively rapid thermal drawdown of the produced water, from 175 to

85°C (345 to 185°F), indicated that the effective heat-transfer area was small, about 8000 m^2 (86 000 ft^2), and essentially confined in a fractured region between the main injection and production zones in the EE-1 and GT-2B wells (Refs. 1-3).

Run Segment 3 (Expt. 186), the High Back-Pressure Flow Experiment[4] was run during September and October 1978 for 28 days. The purpose of this experiment was to evaluate reservoir flow characteristics at high mean-pressure levels. The high back pressure was induced by throttling the production well. As a consequence of these higher operating pressures, the flow impedance was reduced several fold, but as discussed later, the effective heat-transfer area remained nearly the same.

It was discovered during Run Segment 3 that, as a result of deteriorated casing cement, the water injected into EE-1 was flowing in the annulus to depths as shallow as 760 m (2500 ft). This posed a potential danger to the ground-water aquifers and caused high water losses. To alleviate these problems, and also to investigate the feasibility of creating a larger fracture from the same wellbores, the EE-1 casing was recemented near its casing bottom at 2.93 km (9600 ft). An enlarged reservoir was then formed by extending a hydraulic fracture from an initiation depth of 2.93 km (9620 ft) in EE-1, about 200 m deeper than the first fracture in EE-1. The fracturing was conducted in March 1979, with two fracturing experiments. These experiments are referred to as "massive" hydraulic fracturing (MHF) Expts. 203 (March 14) and 195 (March 21). In each experiment, approximately 760 m^3 (200 000 gal) of plain water were injected at a rate of approximately 0.04 m^3/s (600 gpm). The downhole pressure was raised by about 20 MPa (3000 psi). The resulting large fracture (Sec. II) propagated upward to at least 2.6 km (8600 ft). Thus, the new fracture appeared to have a minimum inlet-to-outlet spacing of 300 m (1050 ft), more than three times that of the reservoir prior to refracturing, which suggested that the effective heat-transfer area might be significantly greater than in the first reservoir. Preliminary evaluation of the new reservoir was accomplished during a 23-day heat-extraction and reservoir-assessment experiment that began October 23, 1979. This segment of operation with the EE-1/GT-2B well pair was Run Segment 4, or Expt. 215 (Ref. 5).

The long-term reservoir characterisics were investigated in Run Segment 5, or Expt. 217, which began March 3, 1980. Because of the large size and resulting slow thermal drawdown, a lengthy flow time of 286 days was necessary

to evaluate the reservoir. This experiment, along with its startup phase and the 2-day Stress Unlocking Experiment (SUE) that immediately followed Run Segment 5 are described in Refs. 6-8.

Because of the low power levels produced with these research size reservoirs, no attempt was made during Run Segments 2 through 4 to use the geo-heat for generating electrical energy or for some other useful purpose. Instead, the heat was simply dissipated into the atmosphere by the heat exchanger. However, during Run Segment 5 an electrical generating unit designed and assembled by Barber-Nichols Engineering was incorporated in the circulation loop. This generator extracts energy from the water produced from the reservoir and heats the generator working fluid, Refrigerant 114, which is then expanded through a single-stage turbine. Problems with leakage of the working fluid for the generator prevented sustained operation of the generator, but it did produce a peak power of 60 KWe.

In the 3 years during which these reservoir tests were conducted, our understanding of reservoir behavior has steadily improved. In particular, numerical modeling evolved continuously, so that simplified models that were developed for Run Segment 2 were significantly modified by the time of Run Segment 5. Consequently, the purpose of the present report is twofold: first, to present a convenient summary of all reservoir test results to date, and second, to analyze these results in a consistent manner using our most recently developed models. In conjunction with these new analyses, recommendations for future experimentation in the Phase I reservoir, which are relevant to the future development of the Phase II reservoir, will be presented.

II. GEOLOGY AND GEOMETRY

The subsurface geology at the Fenton Hill HDR site is described in a number of papers. Laughlin and Eddy[9] presented in detail the petrography and geochemistry of the Precambrian rocks encountered by drill holes GT-2 and EE-1. Laughlin[10] reviewed these data, related the geology of the site to the regional geology of the Jemez Mountains, and discussed the relations between the HDR and hydrothermal geothermal systems associated with the Valles Caldera. More recently, Laney et al.[11] and Laughlin et al.[12] integrated new data from EE-2 with the earlier GT-2 and EE-1 data to characterize the Phase II reservoir now under development.

Our knowledge of the Precambrian rocks, which comprise the Phase I reservoir, results from a synthesis of petrographic, geochemical, and structural data collected on cores and cuttings from GT-2 and EE-1 and the results of geophysical logging in the two wellbores. From this synthesis, it is evident that the Precambrian rocks are both compositionally and structurally very diverse and complex. As discussed below, however, the Phase I system was developed in a single, large, homogeneous rock unit within this complex.

Figure 2 presents a schematic of lithology and virgin rock temperatures as a function of depth. After drilling through approximately 730 m (2400 ft) of younger volcanic and sedimentary rocks, within which the geothermal gradient is about 100°C/km, crystalline basement rocks of Precambrian age were encountered. The gradient in the crystalline rocks is about 55°C/km. About 75% of the crystalline rocks from 0.75 to 3 km is made up of very heterogeneous metamorphic rocks (gneisses and relatively minor biotite schist). The gneisses are composed of varying proportions of quartz, plagioclase and alkali feldspars, and biotite. Abundances of these minerals may change abruptly over distances of only a few centimeters. Because of the well-developed foliation, the gneisses are texturally anisotropic. On a larger scale, the anisotropy is enhanced by relatively thin zones of biotite schist that are interlayered with the gneisses. These schists are much finer grained than the gneisses and contain much more biotite. The northeast-striking foliation in these metamorphic rocks probably is the cause for the northwest drift of the GT-2 and EE-1 wellbores observed during their drilling.

Several granitic igneous rock bodies are intrusive into the metamorphic complex. Of relatively minor importance are small dikes of monzogranitic composition. One of these, sampled by a core from GT-2, occurs at a depth of approximately 1305 m and is about 15 m thick. Geophysical logging indicates that two other such dikes were penetrated by GT-2 and EE-1. Analysis of cuttings and cores from EE-2 and EE-3 indicates that compositionally similar monzogranitic dikes are more common at depths greater than 3 km. More significant to the HDR program is a biotite granodiorite body that extends from a depth of 2.59 km to about 3 km. The Phase I system was developed within this rock. This biotite granodiorite is a very homogeneous granitic rock composed principally of quartz, plagioclase and alkali feldspars, and biotite (Table I). Several per cent of the titanium-bearing mineral, sphene, serve to distinguish this rock from other rock units encountered in the section.

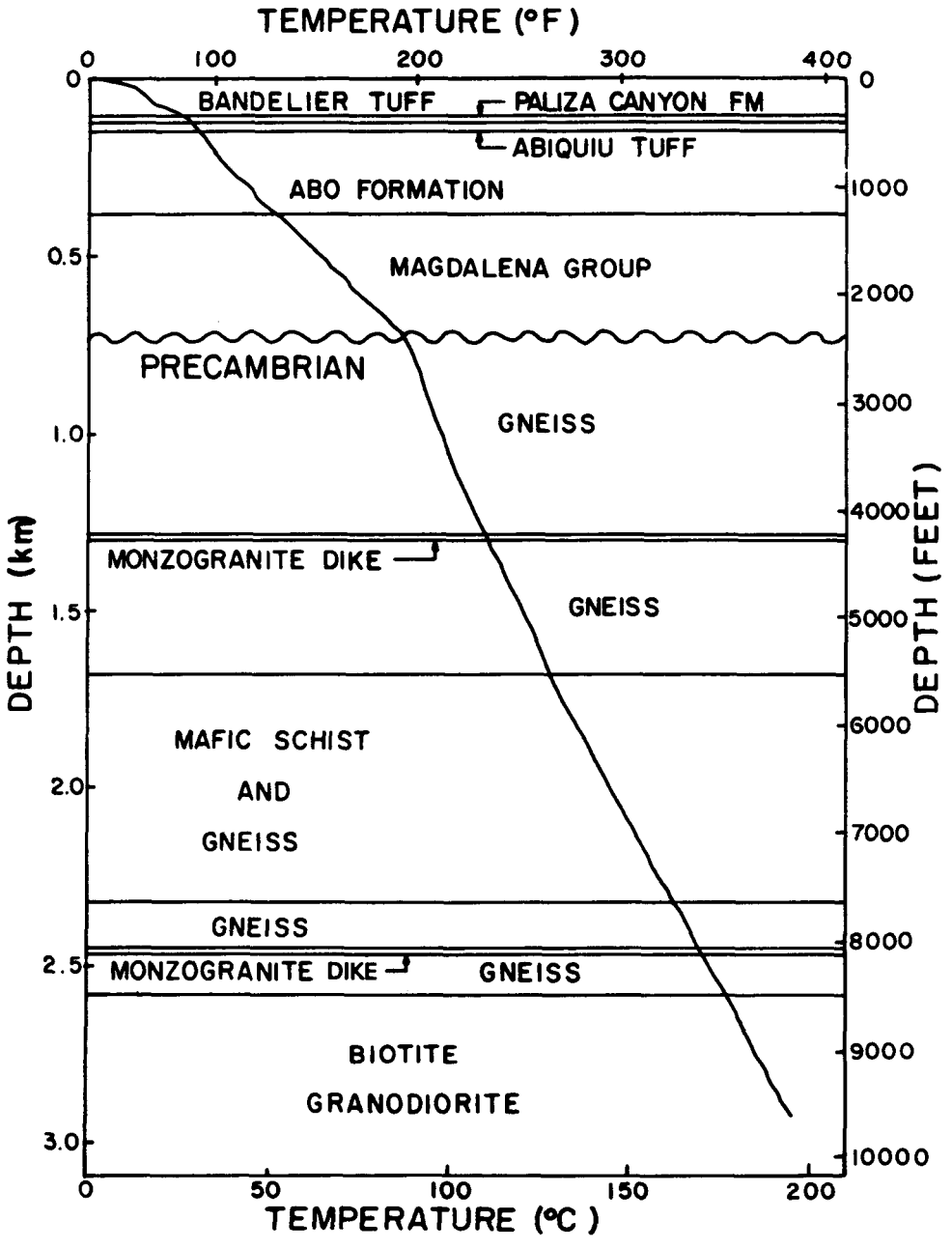

Fig. 2.
Variation of temperature and lithology with depth. The Bandelier Tuff, Paliza Canyon Formation, and Abiquiu Tuff are volcanic rocks of Cenozoic age associated with the formation of the Jemez volcanic pile and caldera. The Abo Formation consists mainly of Permian sandstones and shales; the Magdelena group is composed of the Madera Formation (limestones) and the Sandia Formation (sandstones and limestones) of Pennsylvanian age. The Precambrian rocks consist of granitic gneiss, mafic schist, and biotite granodiorite.

TABLE I

MINERALOGICAL AND CHEMICAL COMPOSITION OF THE FENTON HILL BIOTITE GRANODIORITE

Mineral	Modal Per cent[a]	Oxide	Weight Per cent[b]
Potassium feldspar	19	SiO_2	64.27
Plagioclase feldspar	36	TiO_2	0.95
Quartz	26	Al_2O_3	14.48
Biotite	12	Fe_2O_3	2.96
Sphene	2	FeO	2.92
Other trace minerals	5	MgO	1.39
		CaO	3.11
		MnO	0.09
		Na_2O	3.32
		K_2O	4.23
		H_2O^-	0.07
		H_2O^+	0.98
		P_2O_5	0.57

[a]Average of three samples.
[b]Average of six samples.

Texturally the biotite granodiorite is equigranular and nonfoliated. Geochronological investigations reported by Brookins et al.,[13] and textural evidence indicate that the biotite granodiorite is younger than the metamorphic complex and intrusive into it. Results of chemical analyses of six samples of the biotite granodiorite also indicate that it is very homogeneous and that it can be distinguished on the basis of high TiO_2 and P_2O_5 contents.

The biotite granodiorite, like the other Precambrian rocks at Fenton Hill, contains many joints or natural fractures, which are seen at 0.01- to 0.1-m intervals in cores and are recognized on certain geophysical logs. These joints are almost invariably sealed by a variety of minerals including calcite, alkali feldspar, epidote, and quartz. The sealing processes have been so effective that intrinsic permeability and water losses during flow tests have been extremely low. Apparently seismic activity, which commonly

keeps joints open in natural hydrothermal systems, has been too low in the Fenton Hill area to reopen the sealed fractures.

As mentioned in the introduction, reservoirs were created in the biotite granodiorite at a depth interval of 2.6 to 3.0 km by hydraulically fracturing well EE-1 and sidetracking (deviating) well GT-2 to pass through the fractured region. In our early concept it was believed that the deviated path of GT-2, called GT-2B, failed to intersect the hydraulic fracture directly, but did at least intersect several joints inclined from the vertical, which provided flow communication from the hydraulic fractures initiated from EE-1.

Reservoir geometry can be inferred from several different experiments and a variety of data. The most common data used are those obtained from tracer, spinner, and temperature logs, and heat-extraction experiments. These experiments, together with the expected finding that the minimum earth stress at reservoir depth is in the horizontal direction so that the induced fractures are vertical, have led to the inferred fracture geometry shown in Figs. 3 and 4.

Figure 3 is an early conceptual model of the system showing the small fracture exploited for Run Segments 2 and 3 and the enlarged fracture system of Run Segments 4 and 5. Also shown are the connecting, nonvertical natural joints with a dip of about 60° from the horizontal. Note that the hydraulic fractures are shown to be circular in Fig. 3. This is admittedly speculative. However, unlike oil and gas reservoirs where distinct changes in the lithology (such as upper and lower confining shale layers) result in roughly rectangular fractures, it is thought that the fractures in this HDR system are roughly circular because of the gross homogeneity of the biotite granodiorite. Almost all the heat-transfer area in this model of the system is associated with the hydraulic fractures. The heat-transfer area of the inclined joints, expected to be small, is lumped for computational convenience with the main hydraulic fractures. The independent-fractures model (discussed in Sec. III) is based on this representation of the reservoir. Using this analysis, the area of the first fracture was initially calculated at 8000 m^2, which gives an equivalent diameter of 100 m. Similarly, initial estimates indicate that the larger fracture is 35 000 m^2, or has an equivalent diameter of about 200 m.

Figure 4 is a more recent view of the system. This model is characterized by a multitude of vertically oriented fractures. This view of the reservoir evolved after a detailed analysis of temperature drawdown and recovery

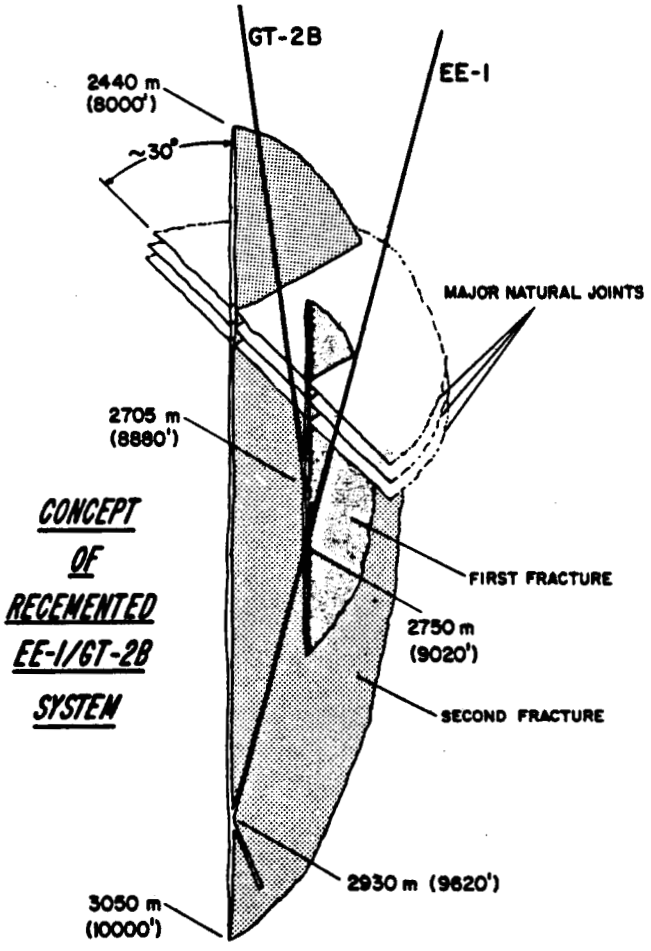

Fig. 3.
Inferred reservoir geometry (early conception).

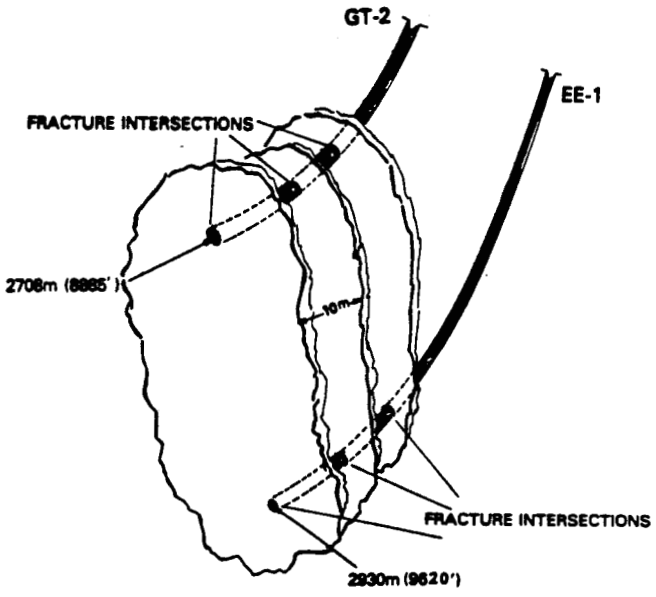

Fig. 4.
Inferred reservoir geometry (present conception).

curves in both wellbores (more details are also given in Sec. III). This model gave a total heat-transfer area for the reservoir of 45 000 m^2.

III. HEAT PRODUCTION AND HEAT-TRANSFER MODELING

During Run Segments 2 through 5, the temperature of the water exiting the reservoirs was measured with a thermistor surveying tool positioned in GT-2B. This tool has a resolution of 0.05°C. Combined with the thermistor is a flow rate sensor, that is, a "spinner," so that both temperature and flow rates of the water exiting the reservoir and entering GT-2B via various natural fractures or joints could be monitored. Cumulative thermal energy extracted from the Phase I reservoir during Run Segments 2 through 5 is illustrated in Fig.

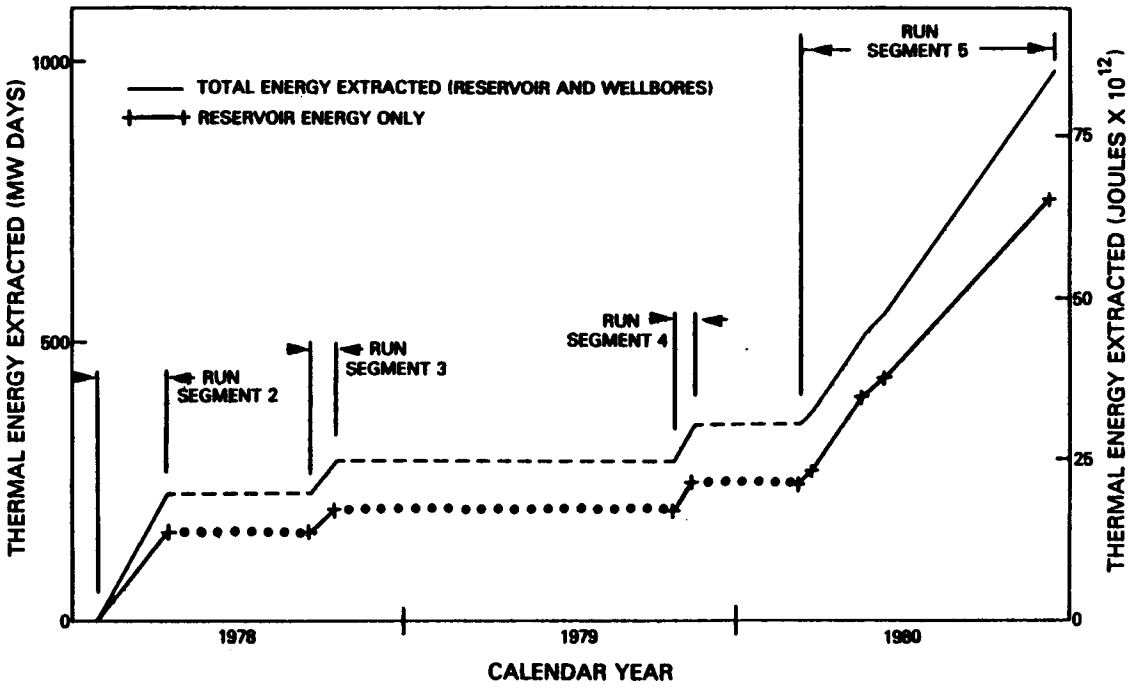

Fig. 5.
Cumulative thermal energy extracted from the Phase I reservoirs, Run Segments 2 through 5.

5. The upper curve depicts total energy produced at the surface. Measured GT-2 production temperatures were used and a constant 25°C reinjection temperature was assumed for EE-1. The lower curve represents energy extracted from flow across the reservoir and excludes contributions from the wells. Based upon wellbore heat-transmission calculations, an inlet reservoir temperature in EE-1 of about 65°C was used when measured downhole temperatures were unavailable. The outlet reservoir temperature was taken from GT-2 temperature logs measured at 2590 m (8500 ft). Average thermal energy extracted at the surface was 3.1 MWt for Run Segment 2, 2.1 MWt for Run Segment 3, 2.8 MWt for Run Segment 4, and 2.3 MWt during Run Segment 5.

Although Run Segment 2 produced thermal energy at the greatest rate, thermal drawdown was quite severe. After 75 days of operation the GT-2 reservoir temperature had dropped from 175 to 85°C. Temperatures during Run Segment 3 ranged from 135 to 98.5°C, while temperatures during Run Segment 4 remained almost constant at 153°C. Finally during Run Segment 5, the initial reservoir temperature of 156°C climbed to about 158°C after 60 days then dropped to about 149°C by the experiment's end (286 days).

The rate of decline, or drawdown, of these temperatures, when analyzed with the heat-transfer models briefly described below, permits estimates of the effective heat-transfer areas of the reservoirs. We say effective because some parts of the total area are either inaccessible to, or inefficiently bathed by, the water flow because of fluid dynamic and geometrical considerations.[14]

Heat-transfer modeling of the reservoirs has been performed with two numerical models. These models have been described in detail previously,[14-16] but a summary is provided here for convenience. Both models use two-dimensional simulators in which heat is transported by conduction within the rock to the fractures. The most recently developed model, which we call the multiple-fracture model, is based upon the geometry of Fig. 4 and assumes that the fractures are parallel rectangles and that flow is distributed uniformly along the bottom of each fracture and uniformly withdrawn from the top of each fracture. The flow is thus one-dimensional, and the streamlines are straight vertical lines. Consequently fluid dynamic considerations do not directly enter into the heat-extraction process -- the sweep efficiency is implicitly assumed to be 100%. However, a rigorous two-dimensional heat-conduction solution is incorporated for the rock between the fractures, and this permits valid consideration of thermal-interaction effects between the fractures. In contrast, the older model (the independent-fractures model), based upon Fig. 3, assumes that the fractures are circular (but other assumptions are permissible) and allows proper local positioning of the inlet and outlets, i.e., the point-like intersection of the injection well with the fracture can be modeled, as can the intersection of the main hydraulic fractures and the slanting joints that provide the connections to GT-2B. However, as was cautioned earlier, while the fluid dynamic effects of the joints/outlets can be faithfully modeled, the heat-transfer effect of the joints cannot; the area of the joints must be lumped with the main fractures. In view of this more faithful representation of inlet and outlets, and the fact that a complete two-dimensional solution to the Navier-Stokes fluid dynamic equations is incorporated, the independent-fractures model results in a more realistic assessment of the effect of fluid dynamics and sweep efficiencies upon heat extraction. The penalty, however, is that in the present two-dimensional version of the code, thermal interaction as the temperature waves in the rock between

fractures overlap cannot be realistically represented, as it is with the multiple-fracture model.

In the most recently conducted experiment, Run Segment 5, it was concluded that while both models are now only two-dimensional, both models predicted reasonably well the overall thermal drawdown. This agreement gives pause to the development of more complicated and expensive three-dimensional models, but nevertheless we are currently developing such models for future reservoirs. In the meantime, we present below our reanalysis of Run Segments 2 through 5 with the most up-to-date, two-dimensional versions of both models. This reanalysis shows that growth of the heat-exchange area occurs not only from pressurization and hydraulic fracturing, as might be expected, but also as a consequence of thermal cooling and thermal stress cracking. Reservoir growth due to thermal cracking during heat extraction was predicted as early as 1972 by Harlow and Pracht,[15] but this is the first time we have been able to detect such growth in the actual drawdown behavior.

A. Independent-Fractures Modeling

The first application of this model was to the first reservoir, when only the smaller hydraulic fracture shown to the right in Fig. 3 existed. This reservoir was tested extensively during Run Segment 2, also referred to as the 75-day test (Ref. 2). Based upon spinner and temperature surveys in the production well, the depths of the intersections of the production well with the slanting joints were estimated as well as the flow rates communicated by each joint. In the calculations, the actual temporal variations of production and injection flow rates were utilized. The fracture inlet temperature was estimated with a separate wellbore heat-transmission calculation.[17] With this information, estimates of the thermal drawdown were calculated with the model for various trial values of fracture radii and vertical position of the fracture inlet. It could not be assumed that the inlet was located at the center of the fracture because the earth stresses increase with depth, so that during its creation the fracture probably grew preferentially in the upward direction. A fracture radius of 60 m with an inlet located 25 m above the fracture bottom resulted in a good fit to the measurements, and, as shown in Fig. 6, the computed thermal behavior was in good agreement with the measured temperature. The temperature shown is the mixed mean reservoir-outlet temperature. That is, the mean outlet temperature is taken as the mean of the joint-outlet temperatures measured in the production well, averaged, or weighted, by the

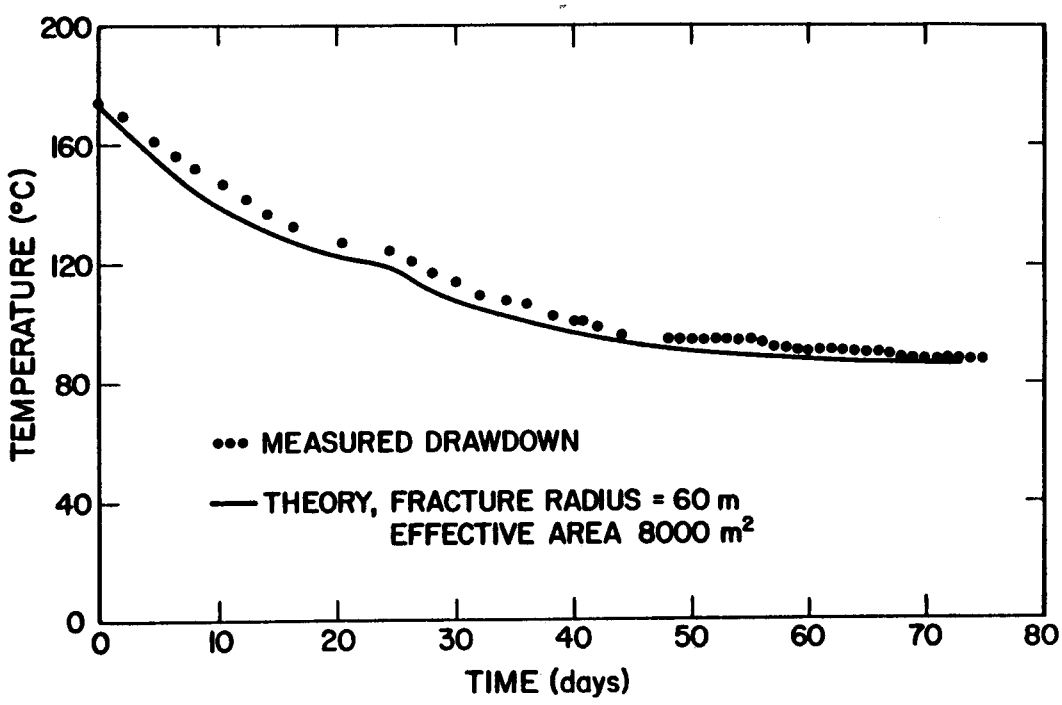

Fig. 6.
Computer model comparison with field data for a single fracture for Run Segment 2.

flow-rate fraction in each joint. This mean outlet-temperature measurement is considered as the best measure of the overall thermal performance of the reservoir and is used, for this model, to describe not only the old reservoir, but also below, the enlarged, two-fracture reservoir. However, as will be indicated later, one of the strengths of the newer, multiple-fracture model, is that the temperatures of the individual joints, as well as the mean temperature, are also modeled realistically. A radius of 60 m, as indicated by the fit to the data in Fig. 6, implies a total fracture area (on one side) of 11 000 m^2; however, because of hydrodynamic flow sweep inefficiencies the net area effective in heat exchange was only 8000 m^2 during Run Segment 2. Unlike the newer model, we were unable, with the independent-fractures model, to obtain a clear-cut indication of thermal growth from the drawdown data of Run Segment 2. The very low rate of drawdown in the later period of the test prevented resolution of any potential area increase.

Six months after the conclusion of Run Segment 2, Run Segment 3 (the high back-pressure experiment) was conducted in October of 1978. The purpose was to examine reservoir behavior under conditions of high mean-fracture pressure.

The test duration was short, less than 1 month, but the thermal drawdown suggested that, according to the independent-fractures model, the effective heat area was nearly the same. However, flow rate (spinner) surveys in GT-2 indicated that because of the higher pressure level most of the flow was entering GT-2B at positions that averaged 25 m deeper than during Run Segment 2. In effect the reservoir flow paths were shortened by 25 m, some 25%. A reduction of at least 25% in heat-transfer area would have been expected because this vertical shortening would also result in horizontal contraction of the streamlines, and yet the area estimated from actual drawdown was about the same. It was concluded that while pressurization did indeed result in partial short circuiting of the streamlines, it also resulted in a notable decrease in impedance, which afforded better fluid sweep and bathing of the remaining area. This impedance change is described in more detail in Sec. V.

As described in Sec. I, the reservoir was enlarged during the fracturing operations of 1979, the MHF Expts. 195 and 203. Approximately 760 m^3 (200 000 gal) of water were injected into the reservoir during each experiment, and the pressure was raised by 20 MPa (3000 psi). For the independent-fractures model the enlarged reservoir is portrayed as two fractures, the old one operative in Run Segments 2 and 3, and a new and larger one shown to the left in Fig. 3. The enlarged reservoir was evaluated during Run Segment 4,[5] and Run Segment 5.[7] To summarize the Run Segment 4 studies, it was found that the old fracture had an effective heat-transfer area of 15 000 m^2 and the new fracture had an effective area of at least 30 000 m^2. We say at least because the heat-extraction period was only 23 days, far too short to result in significant depletion of the new fracture. The area determined in Run Segment 4 for the old fracture was at least twice that determined in Run Segment 2. This trend of increasing area is now attributed to thermal stress cracking effects.[18]

Better estimates of the total effective heat-transfer area of both fractures were obtained in Run Segment 5, during which the thermal drawdown was only 8°C. This drawdown, and the model predictions for several values of the combined areas, are shown in Fig. 7. The data ranges shown should not be interpreted as error bars. Instead, the ranges merely reflect the differences that occur if the thermal decline is measured with respect to the initial mean reservoir-outlet temperature, or, instead, with respect to the highest mean outlet temperature observed. The mean outlet temperature actually increased

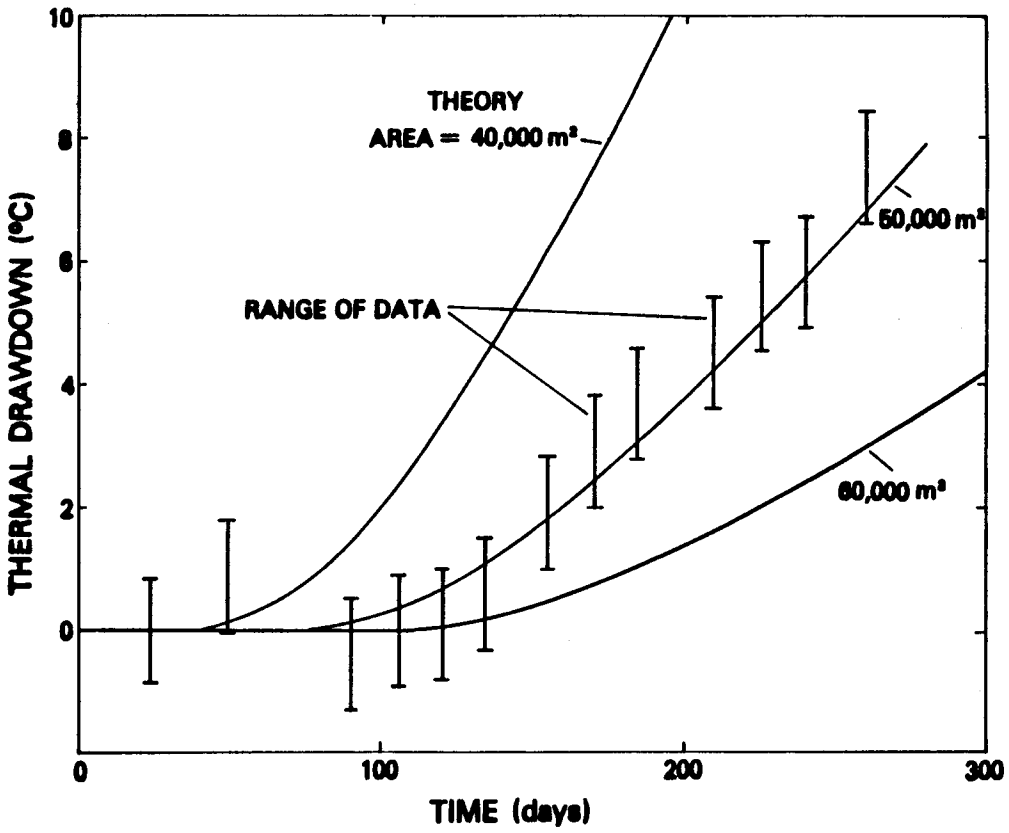

Fig. 7.
Computer model comparison of field data with independent fracture model for Run Segment 5.

slightly during the early portion of Run Segment 5. This temporary increase is due to transport of deeper, hotter water to the production well, as well as to some interaction of the fractures. For simplicity the effect was neglected in the independent-fractures model as it is fairly small, less than 2°C. As shown in Fig. 7, the data are fit very well by a model with a combined area of 50 000 m^2, some 5000 m^2 greater than the area tentatively estimated from the very small drawdown during Run Segment 4.

A summary of the heat-exchange areas determined with the independent-fractures model is presented in Fig. 8. As can be seen, a steady increase, from 8000 to 50 000 m^2, is indicated. This trend is supported not only by the newer modeling discussed next, but also by reservoir tracer experiments presented in Sec. IV. As indicated by the question marks in Fig. 8, the area increase due to the MHF experiments (195 and 203), is uncertain. The heat-transfer area was not measured until the later stages of Run Segment 4. Unfortunately, the first stages of Run Segment 4 were fracturing operations in

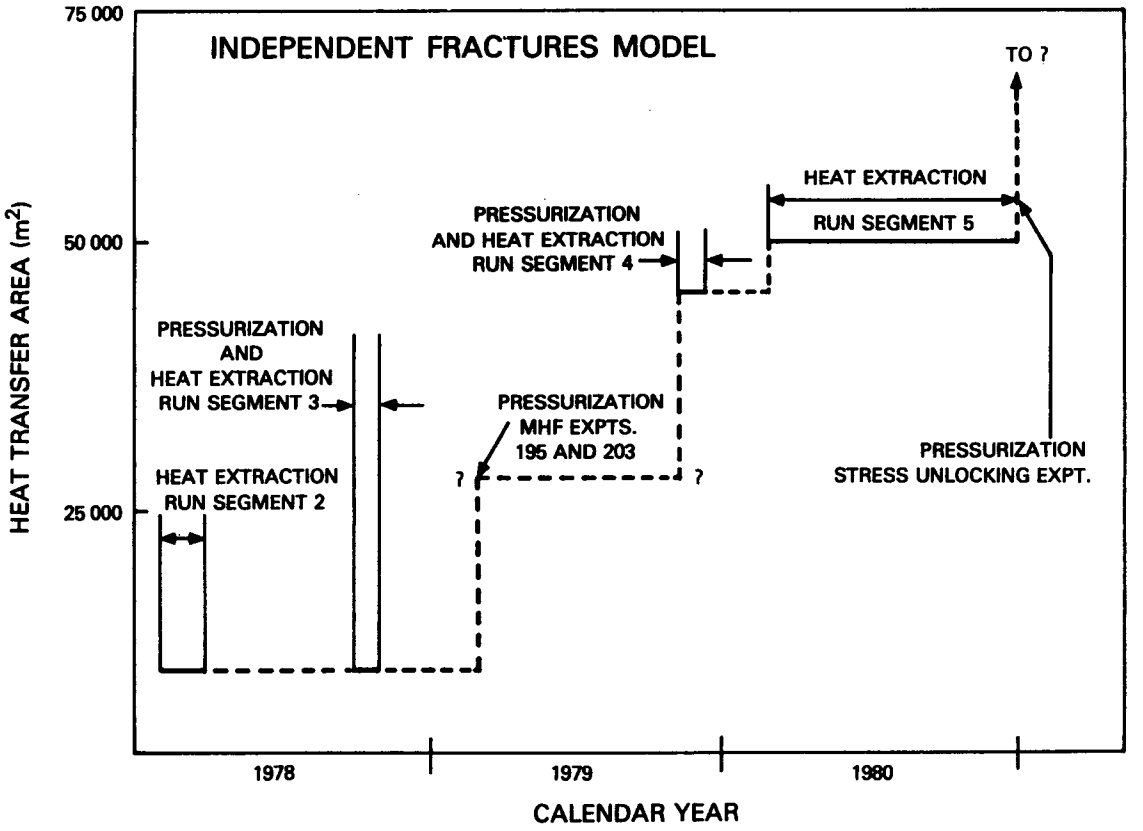

Fig. 8.
Heat-transfer area growth determined by the independent fractures model in the Phase I reservoirs during Run Segments 2 through 5.

their own right, about 3 MPa (500 psi) lower in pressure, but seven times the injection volume of MHF Expts. 203 and 195. Consequently, the area increase measured in Run Segment 4 is due to the combined effects of all the fracturing operations, and cannot be individually ascribed to the separate operations. This uncertainty will also be apparent in the multiple-fracture modeling and the reservoir-tracer experiment.

B. Multiple-Fracture Modeling

The mean reservoir-outlet temperature as measured at 2620 m (8600 ft) in GT-2B during Run Segment 2, is replotted in Fig. 9 along with model fits that invoke an increasing heat-exchange area. The following procedure was used to fit the data.

- The measured GT-2B flow rate and estimated reservoir inlet temperature were programmed as functions of time.
- The initial fracture area was adjusted to obtain the best fit at early times.

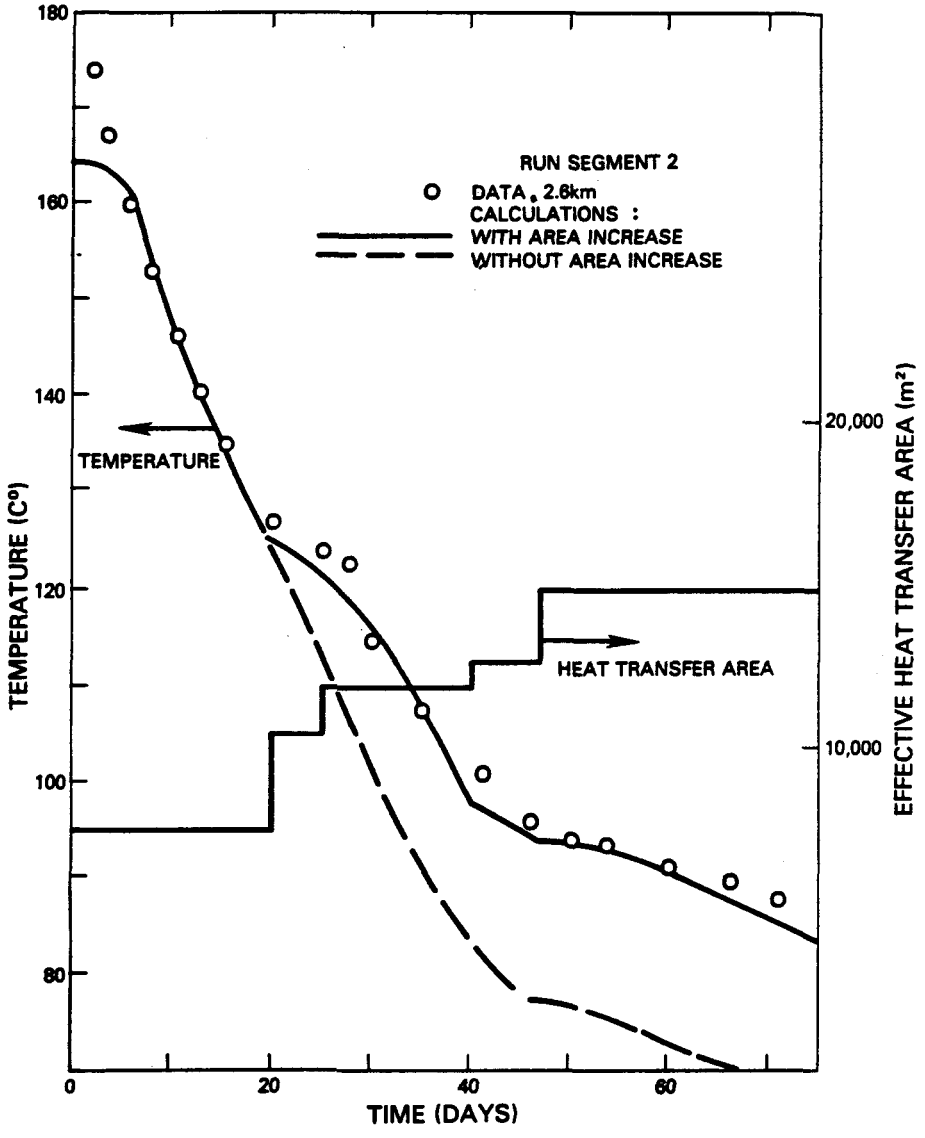

Fig. 9.
Computer model comparisons of field data with programmed increases in heat-transfer area for Run Segment 2.

- The fracture area was allowed to increase so as to provide a good fit to the remaining data. For computational simplicity, the area increase was assumed to occur in discrete steps rather than in a smooth, say piece-wise linear, fashion.

The resulting step increases in the area necessary to fit the data are also shown in Fig. 9.

For the high back-pressure experiment, Run Segment 3, measured downhole inlet temperatures are available, as are measured GT-2B flow rates. The same procedure was followed to fit the drawdown and infer heat-exchange areas. The

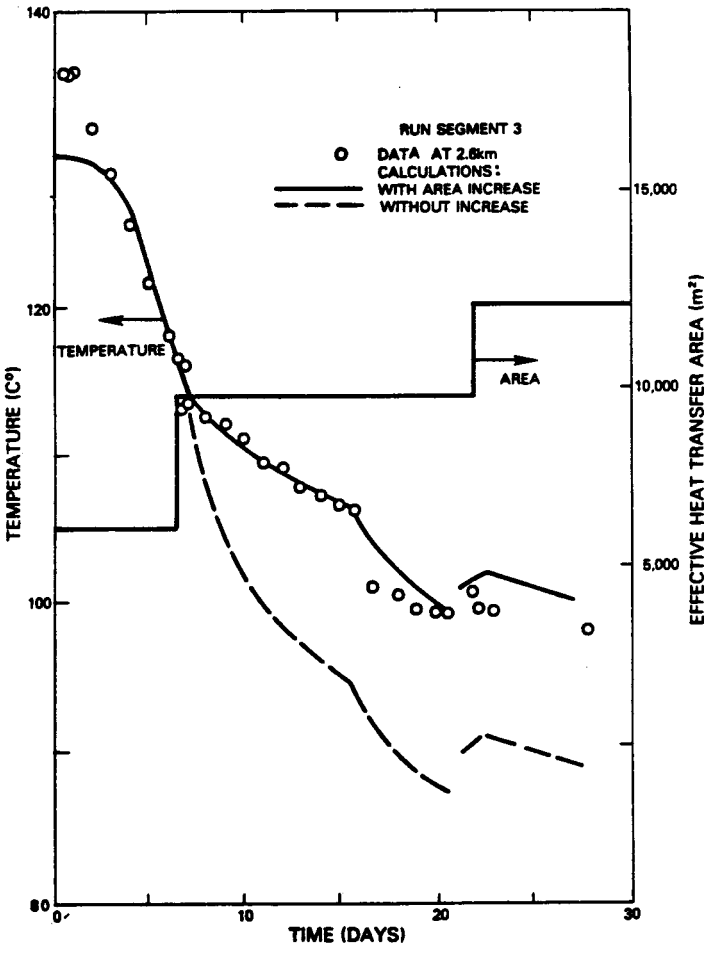

Fig. 10.
Computer model comparisons of field data with programmed increases in heat-transfer area for Run Segment 3.

results are presented in Fig. 10. The cases of constant or increasing area are compared. As indicated earlier, the independent-fractures model was not able to detect any increase in the effective heat-transfer area during actual drawdown. The present analysis indicates that the heat-transfer area could have increased by a factor of two during either Run Segment 2 or 3. Furthermore, this analysis assumes that the temperature of any new area is close to that of the existing reservoir. If the new area is being produced by thermal stress effects, it most likely occurs in the coldest portions of the reservoir, and its temperature would consequently be less than the average reservoir temperature. The actual area increases would even be larger than estimated here.

Similar modeling was carried out for Run Segments 4 and 5. Figure 11 summarizes the growth of the heat-exchange area, according to the

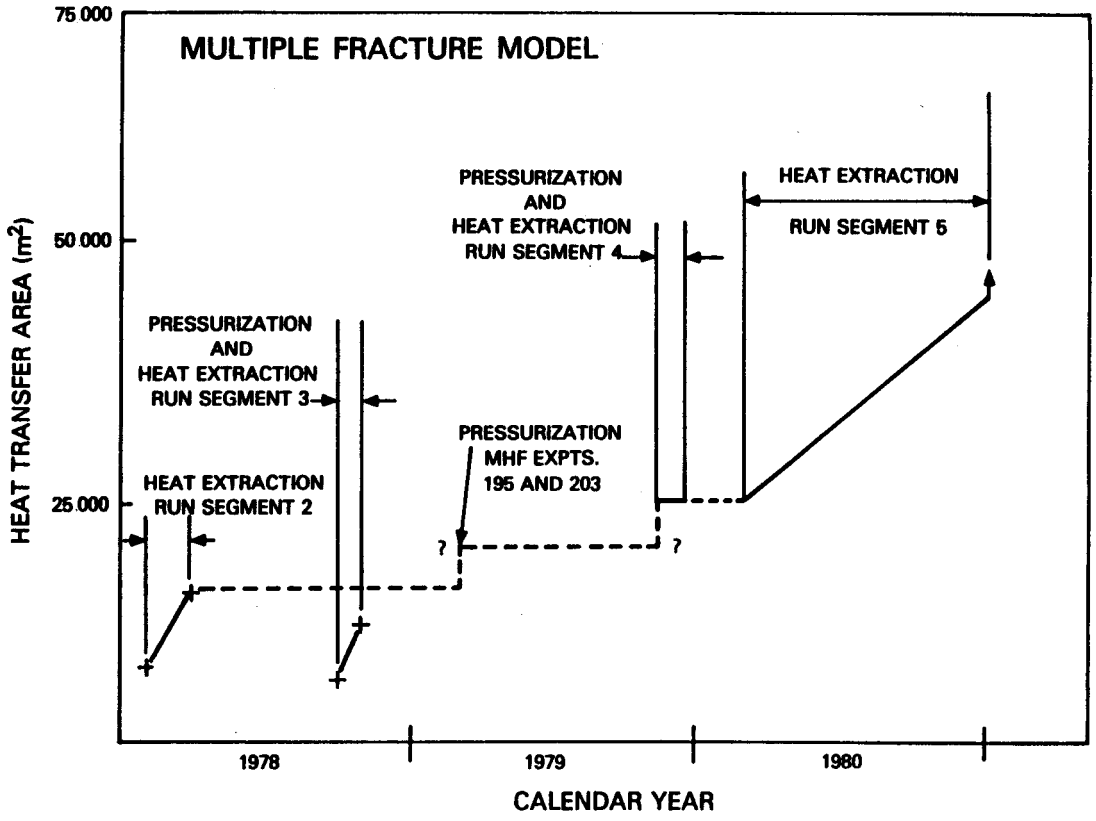

Fig. 11.
Heat-transfer area growth determined by model fits to drawdwon data and wellbore temperature logs in the Phase I reservoirs during Run Segments 2 through 5.

multiple-fractures model, throughout Phase I. The general similarity with the summary of the independent-fractures model, Fig. 8, is noted, but there are differences in detail. The initial area of 7500 m^2 was established by many pressurizations and some cooling. This area grew to 15 000 m^2 in Run Segment 2. As indicated earlier the high back pressure of Run Segment 3 caused a redistribution of flow resulting in fluid dynamic short-circuiting. However, unlike the independent-fractures model, the new model indicates that the initial heat-exchange area was actually less than that of Run Segment 2, starting at 6000 m^2; but it then grew to 12 000 m^2 during the 28-day test. The system was pressurized to high pressures several times during MHF Expts. 203 and 195 and Run Segment 4 but no area or volume measurements were made until Run Segment 4. After Run Segment 4, the EE-1 temperature logs indicated that between 6000 and 9000 m^2 had been added to the lower part of the reservoir by the recementing and pressurization prior to and during Run Segment 4. This increased the

measured heat-exchange area to between 21 000 and 24 000 m^2. The area measurements during Run Segment 5 are somewhat uncertain. The best estimates are that the heat-exchange area was greater than 45 000 m^2 at the end of the experiment. The lack of recovery of the outlet temperature indicates that the additional area is in the depleted upper half of the reservoir or was partly added to the lower half as Run Segment 5 proceeded.

C. Comparison of Effective Heat-Exchange Areas With Other Reservoir Areas

Throughout the development of the reservoir, the heat-exchange area has remained small compared to areas obtained from other methods. Table II lists some of these area estimates. The extremely large inflation areas based upon fracture pressurization and inflation are obtained from total injected volumes divided by the effective opening, or aperture, of the fractures. These apertures are discussed below. The actual area associated with the inflation volume could be larger, as some of the water must be in small-scale porosity with smaller apertures. Most of this area cannot be expected to participate in heat exchange.

The diffusion area is obtained mainly from water-loss data. The assumptions used to obtain this area are discussed in Ref. 19. The seismic area is the vertical projection of the locus of seismicity (see Sec. VIII) multiplied by N, the number of fractures in the microseismic volume. For N = 3, as

TABLE II

COMPARISON OF RESERVOIR FRACTURE AREAS
Area (m^2)

Segment	Inflation[a]	Seismic	Diffusion	Vent[b]	Heat Transfer
1		>20 000			
2	5×10^6		~250 000	40 000	7 500
					15 000
3	5×10^6				6 000
					12 000
4		75 000 x N			>21 000
5	20×10^6	90 000 x N	~350 000	>250 000	37 000
					45 000

[a] 1-mm aperture
[b] 4-mm aperture

suggested by the multiple-fractures model, the areas are very close to the diffusion area.

Yet another area can be obtained from the volume of water vented at high flow rates after the system has been pressurized for a long time. The higher vent rates are assumed to come from a large low-impedance system before the decreasing internal pressure closes the fractures. The vent areas in the table are for a fracture system with an aperture, discussed below, obtained from the heat-exchange areas and modal tracer volumes.

The heat-exchange areas, as determined with the multiple-fractures model discussed previously, are in the final columns of the table and are seen to be small compared to the other area estimates. This indicates that only a small portion of the pressurized fracture system is being utilized as heat-exchange area.

The inflation and vent areas were obtained from volume measurements. In each case an upper limit to the aperture was used so that the calculated areas would be lower limits. For the inflation areas a nominal 1 mm was chosen because the larger, uncooled fracture system into which water is forced during inflation (no circulation of water because the production well was shut-in) should have a smaller aperture than the smallest estimates. Pressure-transient testing[19] of the fracture system effective in heat exchange gives an estimate of 1 to 2 mm for the aperture of the active heat-transfer region, whereas Run Segment 2 tracer modal volumes (Sec. IV) and heat-exchange areas provide an aperture estimate of ~1 to 5 mm for the heat-exchange region. Consequently, a nominal 1 mm was chosen for the larger and, essentially, still undeveloped reservoir. Turning now to the area estimate based upon the venting volume, the apertures associated with the low-impedance vent volume should be the same as or smaller than the apertures off the internally depleted, active heat-transfer regions of the reservoirs. The largest aperture estimates for the depleted reservoir were obtained at the end of Run Segment 5 when the modal volume and heat-exchange areas gave apertures of about 4 mm.

IV. TRACER STUDIES AND FRACTURE VOLUME GROWTH

The main objectives of reservoir tracer studies are to assess the volume changes associated with the creation of the Phase I system and to determine dynamic behavior of the system volume as the system undergoes long-term heat extraction. Two tracers were used in these studies. The first is a visible

dye, sodium fluorescein, which is monitored in the produced fluid with a UV spectrophotometer. The other tracer, radioactive Br^{82} (half life equals 36 h) present as ammonium bromide (NH_4Br^{82}), is monitored in the produced fluid with a flow-through gamma counter specially fabricated for this use. The radioactive tracer is not temperature sensitive and therefore does not undergo thermal decomposition as does the sodium fluorescein in the higher temperature portions of the reservoir. Flow conditions and preliminary results of tracer tests from the Phase I system are presented in Table III. In this table, the definitions of modal volume, integral mean volume and variance are the same as those presented by Tester et al.[20] The fracture modal volume is simply the volume of fluid produced at GT-2B between the time the tracer pulse was injected and the time the peak tracer concentration appeared in the produced fluid. The wellbore volumes are subtracted from the total volume produced to give the true fracture modal volumes. The integrated mean volume is obtained by integrating the tracer concentration-time curve at the reservoir exit. As described below, the modal volume is considered the most reliable indicator of reservoir volume change. Large changes in the modal volume are observed after the hydraulic fracturing of the system between Run Segments 3 and 4 and during the SUE, which followed Run Segment 5. SUE was conducted on December 9 and 10, 1980, and the volume change was evaluated with a tracer experiment on December 12, 1980.[8]

The integral mean volumes show a regular increase during Segment 2; however, the integral mean is strongly affected by the volume of fluid produced during a given experiment. During Run Segments 2 and 4, the length of time a given experiment could be run was determined largely by the limit of detection of sodium fluorescein. The highly increased sensitivity of the method for analyzing Br^{82} over that for sodium fluorescein is responsible for longer tails on the Br-tracer experiments. Dye-tracer experiments typically end when the dye concentrations in the produced fluid can no longer be measured (typically <1400 m^3 total produced volume at GT-2B). Bromine-tracer experiments, on the other hand, have continued to 4140 m^3 without completely reaching background. Integration of the long tails of the concentration-time curves biases both the integral mean volume and the variance to higher values. To eliminate the effect of this bias, Tester et al.[20] truncate the integration when 90% of the tracer has been recovered. Variances of the distributions were calculated for the fully integrated distribution and the 90% trimmed mean, and these

TABLE III

SUMMARY OF FLUORESCEIN DYE AND Br^{82} TRACER EXPERIMENTS IN THE PHASE I EE-1/GT-2B FRACTURE SYSTEM

Experiment	Elapsed days	p^g_{EE-1} MPa	p^g_{GT-2} MPa	$\bar{Q}$ $10^3 m^3$ [a]	$\dot{q}_{GT-2}$ $10^{-3} m^3/s$ [b]	$C_f V_f$ tracer feed 10^4(ppm) liters (c)	$\dot{q}_{loss}$ $10^{-3} m^3/s$	Tracer recovery %	Average fluid production temp. °C	Mean <V> m^3	Median [V] m^3	90% Trimmed mean |V| m^3	Variance σ^2_θ	Variance σ^2_θ (90%)	(d) Pe^{*-1}	Mode $\hat{V}$ m^3	Total fluid vol. measured during tracer test	Incremental Thermal energy extracted 10^{12} J	$\hat{V}/t=0$ m^3
ORIGINAL RESERVOIR																			
Segment 2 (75 day)																			
Phase 1-1 (2/9/78)	8	8.8	1.1	8.0	7.25	7.57	1.30	69	150	34.4	25.6	29.3	0.65	0.44	0.591	11.4±1.1		2.29	
Phase 1-2 (3/1/78)	28	8.5	1.1	26.1	13.1	7.57	0.60	65	110	37.5	28.9	30.9	0.62	0.43	0.942	17.0±1.5		7.16	10
Phase 1-3 (3/23/78)	50	6.6	1.1	57.2	13.9	7.57	0,75	71	95	54.7	45.1	46.3	0.51	0.42	0.944	22.7±2.3		12.90	
Phase 1-4 (4/7/78)	65	5.9	1.1	75.7	15.5	7.57	0.18	>65	90	56.2	48.4	49.2	0.47	0.39	1.120	26.5±2.7		16.40	
Segment 3 (28 day)																+5.7			
Phase 1-5 (9/28/78)[i]	10	9.3	9.7	9.0	7.7	7.57	3.17	60	111	33.1	24.7	26.6	0.75	0.56	0.358	3.8-1.9		1.01	
Phase 1-6 (10/13/78)[h]	25	9.3	9.7	26.3	9.3	11.36	3.17	74	98	56.5	46.5	48.1	0.45	0.36	0.306	11.4±1.5		3.36	2.5
Phase 1-7 (10/16-78)[k]	28	9.3	1.7	~30.0	15.7	11.36	4.28	33[e]	-	49.6	40.5	41.8	0.49	0.38	0.347	20.8±1.9		3.70	
ENLARGED RESERVOIR																			
Segment 4 (23 day)																			
215-1 (10/26/79)	-	17.2	1.1	1.3	6.4	11.36	8.70	13(25)[f]	153	207.	192.	184.	0.26	0.22	0.195	136. ±19	469	-	
215-2 (10/29/79)	0	17.2	10.3	6.1	8.1	11.36	14.00	18	154	230.	211.	209.	0.17	0.12	0.360	144. ±19	619	-	120
215-3 (11/2/79)	2	9.3	1.1	9.5	6.6	45.42	1.13	27	153	262.	216.	243.	0.38	0.34	0.281	121. ±11	570	0.37	
215-4 (11/12/79)	12	9.3	1.1	16.2	6.4	45.42	1.27	25	153	283.	236.	263.	0.32	0.28	0.310	129. ±11	662	2.24	
Segment 5 (282 day)																			
217-A1 (4/16/80)	38	9.8	1.3	13.1	6.2	45.42	0.90	>57	158	404.4	341.1	500.	0.45	0.44	0.760	155. ±10	1440	5.9	
217-A2 (5/9/80-Br)[j]	61	9.5	1.3	26.5	5.9	38.4mCi[l]	0.50	-	158	1100.	1072.	941.	0.53	0.52	-	161. ±4	3030[m]	9.9	151
217-A3 (9/3/80-Br)	178	8.8	1.3	74.0	5.7	383.0mCi	0.38	-	154	1311.	1245.	1274.	0.56	0.54	-	178. ±4	4140[m]	27.1	
PreSUE 217-A4 (12/2/80-Br)	268	8.5	1.1	121.0	5.1	519.0mCi	2.30[o]	-	149	581.[n]	541.	525.	0.40	0.38	-	187. ±10	~310[n]	39.9	
PostSUE 217-A5 (12/12/80-Br)	278	8.4	1.3	126.0	8.1	377.0mCi	0.90[o]	-	149	1118.[n]	965.	1009.	0.46	0.42	-	266. ±4	2690[n]	41.2	

[a] 1 gal = 3.785 liters = $3.785 \times 10^{-3} m^3$
[b] 1 gpm = 6.31×10^{-2} liters/s = 6.31×10^{-5} m^3/s
[c] includes diffusional loss and leaks
[d] $Pe^{*-1} = D/u\ell$ = inverse dispersional Peclet number for single 1-D zone fit
[e] spectrophotometer error possibly explains low recovery
[f] 25% recovered after switch to high backpressure in GT-2B
[g] surface pressures not buoyancy corrected
[h] volume correction added 7.344 m^3 (1940 gal) to eliminate negative volumes (early arrivals)
[i] volume correction added 3.937 m^3 (1040 gal) to eliminate negative volumes (early arrivals)
[j] tracer used Br^{82} in place of Na-fluorescein
[k] 10/26/78 test actually during exp. 190 at LBP
[l] millicurie (mCi) strength of feed at injection
[m] corresponds to first arrival of tracer
[n] exp. terminated before tail of distribution
[o] includes annulus leak

values are given in Table III. The variances for the full and the 90% trimmed distributions still show the effects of the long tails; however, the flow distribution associated with low back-pressure operation does not change drastically even after the hydraulic-fracturing episodes. This fact is most clearly shown in Fig. 12 where normalized tracer concentrations from Run Segment 5 are plotted vs produced volume (the volume produced from the time of reservoir injection). Because of the inconsistency in the calculated integral mean volumes, the concentration normalization is performed relative to the modal volume, $\overset{\circ}{V}$:

$$C_\theta = C_i \Big/ \left[\frac{1}{\overset{\circ}{V}} \int_0^\infty C_i dV \right] .$$

The really significant difference among the Segment 5 tracer experiments shown in Fig. 12 is the drastic increase in modal volume due to the SUE experiment. However, the mode also increases regularly with time due to heat-extraction. Apparently the volume of the system increases systematically even though the

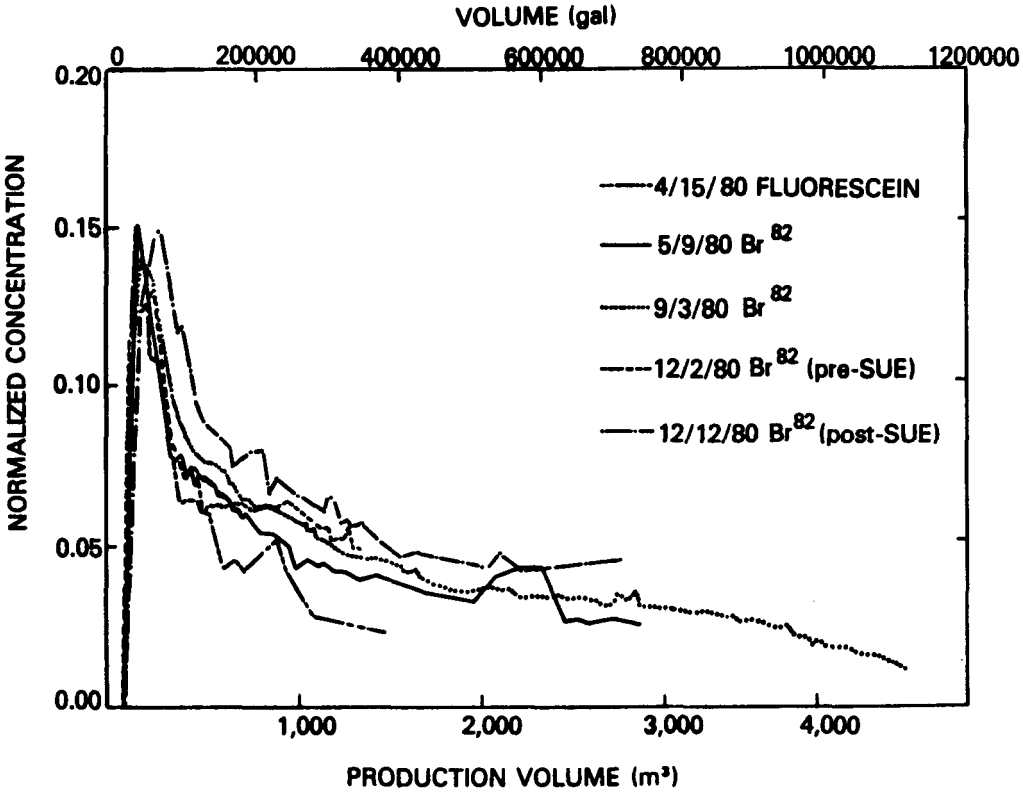

Fig. 12.
Variation of normalized tracer concentrations with produced volume of fluid.

shape of the distribution remains fairly unchanged even after the SUE (see Table III).

A complete review of the tracer-test data from Segments 2 through 5 has revealed pertinent information regarding the growth of the reservoir due to heat extraction and pressurization effects. The reservoir growth due to heat extraction is, to be precise, really a thermal-contraction effect -- as the rock surrounding the fractures shrinks, the fractures, and consequently, the measured volumes, expand. Ultimately, we would like to correlate measured tracer volumes with effective heat-transfer surface. In addition, the interpretation of tracer volume changes could be used to develop improved methods of reservoir operation -- for example, remedial pressurization for stress relief such as SUE, or a huff-puff operation mode in contrast to our normal (stress-constrained) continuous mode of extracting heat (see Sec. X).

Figure 13 is a linear plot of modal-volume increase ($\Delta\mathring{V}$) as a function of net thermal energy* extracted from the reservoir (ΔE) while Fig. 14 shows the same data on a logarithmic scale. Essentially identical linear behavior is observed for the low back-pressure experiment, Run Segment 2, of the original reservoir and the low back-pressure experiment, Run Segment 5, of the enlarged system. In spite of nonlinear coupled effects of thermal contraction, pore and fracture inflation due to sustained pressurization, and local irreversibilities resulting in fracture propagation, a simple correlation between ΔV and ΔE exists. Furthermore, this simple relationship persists even in the presence of the confining stresses surrounding the active reservoir, which induce a constrained behavior. The slope of the line for low back pressure is only about 10% of what would be expected for free thermal expansion ($\Delta V = [\alpha_v/(\rho C)_r]\Delta E$) in a stress-free environment. Values of $\alpha_v = 24 \times 10^{-6} K^{-1}$, $C_r = 1000$ J/kgK and $\rho = 2700$ kg/m^3 were used to represent the granite matrix. For practical purposes, the region between the low-pressure data and the free thermal volume lines defines an envelope of reservoir operating conditions. As stresses are relieved, for example during SUE, or the high back-pressure test of the original reservoir (Run Segment 3), or the high-pressure, hydraulic-fracturing stage at the beginning of Run Segment 4, one moves away from the normally constrained condition toward the free thermal expansion line.

*Excludes energy contributions from the wellbores.

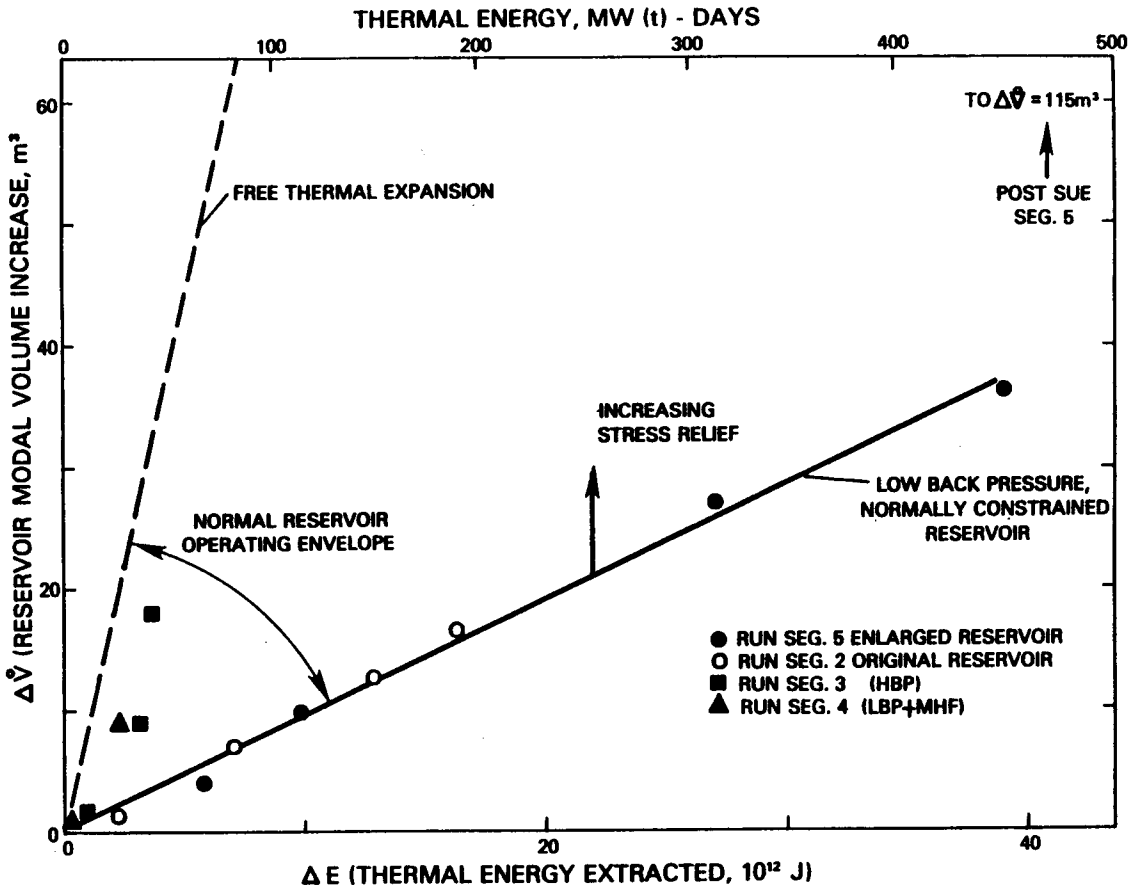

Fig. 13.
Increase in tracer modal volume as a function of thermal energy extracted.

Perhaps the most promising aspect of the tracer tests is their potential for estimating the effective heat-transfer surface area of a reservoir. This becomes clear when the modal volume (plotted vs time in Fig. 15) is compared to the corresponding heat-transfer area (plotted vs time in Figs. 8 and 11); the similarities of the growth of area and volume are quite striking. This can be quantified by considering the relationships between area, volume, and aperture (or effective fracture opening). The volume, V, is simply the product of the area, A, and the mean aperture, w:

$$V = A \cdot w \quad .$$

During heat extraction and/or pressurization, the area and aperture can both vary; therefore the volume is a function of two variables rather than one. For constant aperture, the tracer volumes should scale directly with

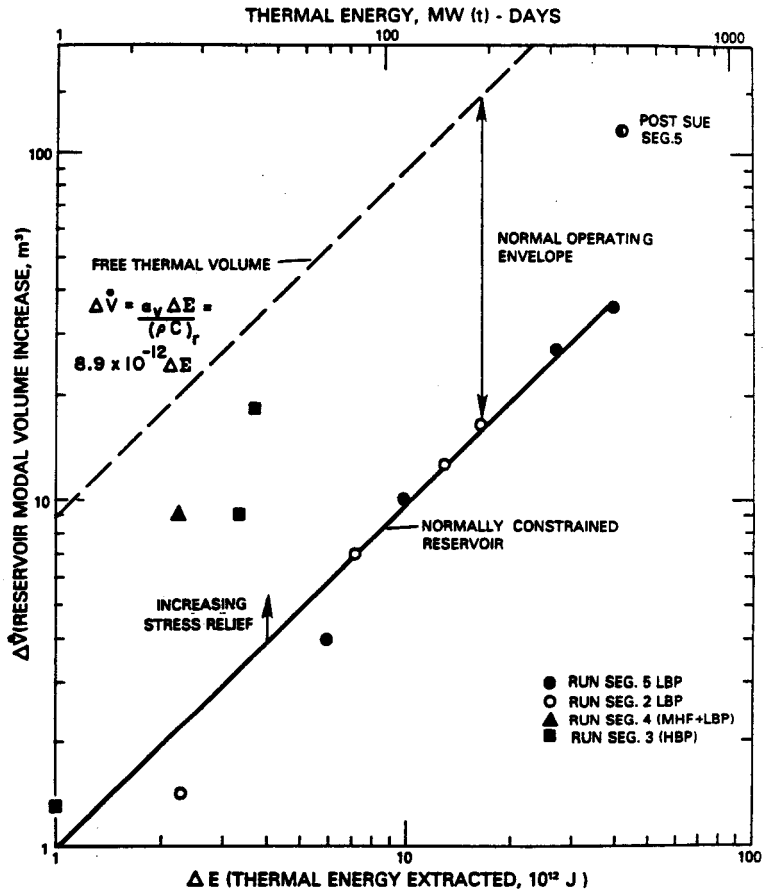

Fig. 14.
Increase in tracer modal volume as a function of thermal energy extracted.

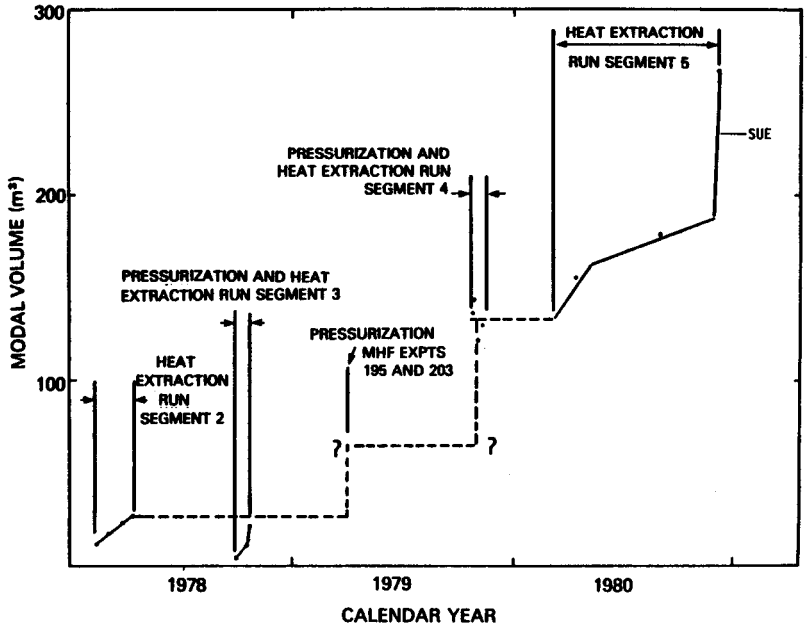

Fig. 15.
Growth of tracer modal volume in the Phase I reservoirs during Run Segments 2 through 5.

heat-transfer area. A suggestion of this behavior is seen in the data from Run Segment 2, shown in Fig. 16, where the area vs modal-volume curve has an intercept that corresponds to a constant 1.7-mm aperture. Subsequent pressurization has apparently increased the aperture. Because only minimum estimates of the heat-transfer area are available for two of the measured volumes in Run Segments 4 and 5, not all of the tracer data can be used in this figure. It is likely that the data from Run Segment 5 would also fall upon a line of constant aperture, in which case, the mean fracture aperture would be roughly 4 mm. There is insufficient information available to provide upper bounds for the heat-transfer area from Run Segment 5, so the correlation between heat-transfer area and modal volume is inferred by analogy with Run Segment 2. Further development of this empirical correlation could provide a direct and

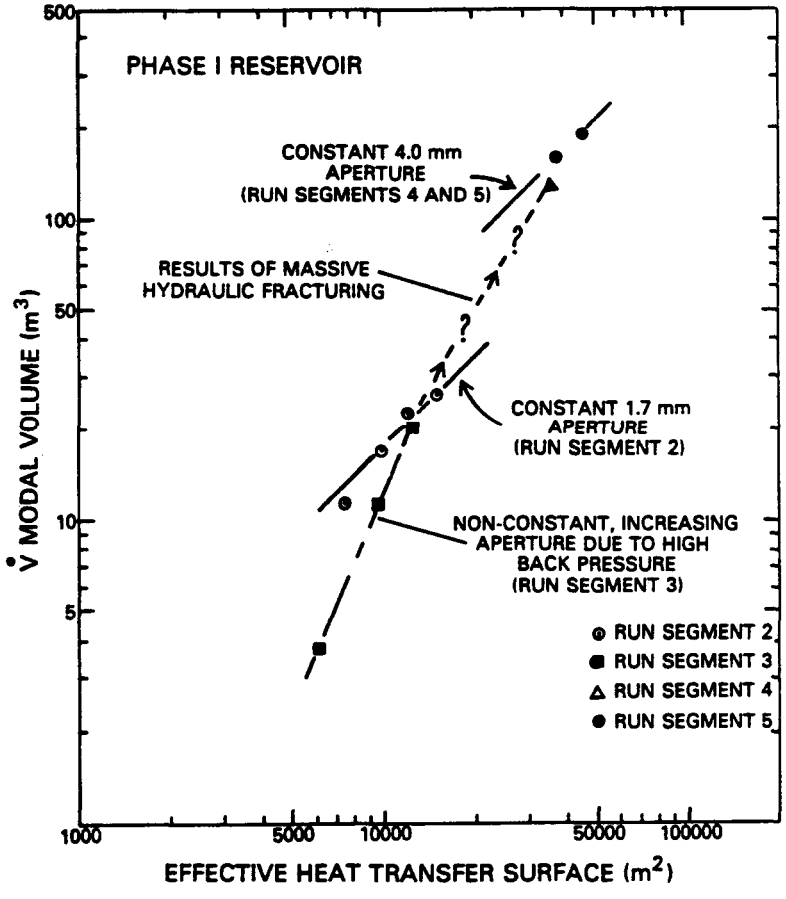

Fig. 16.
Preliminary correlation of increases in effective heat-transfer surface area with modal volume increase in the Phase I reservoir.

independent method of determining reservoir heat-transfer area without requiring thermal drawdown, which is time consuming and expensive to obtain, particularly so for the larger Phase II reservoir under development.

V. IMPEDANCE CHARACTERISTICS

The impedance of a circulating geothermal reservoir is usually defined as the pressure drop between the inlet and outlet of the fracture caused by flow in the fracture, divided by the exit volumetric flow rate. Its units are pressure-s/volume, and in this report we typically use Giga Pascals per cubic meter per second (GPa s/m^3) or in English customary units, pounds per square inch per gallon per minute (psi/gpm).

Because pressures are usually measured at the surface, a "buoyancy" correction should be made for the difference in hydrostatic pressures in the hot production well and the cold injection well. The depth at which this correction is calculated corresponds to the bottom of the injection well, that is, buoyancy inside the fracture is included in the hot leg. Accurate buoyancy calculations from measured or calculated wellbore-temperature profiles were used in the actual calculation of impedances given below. In reviewing the impedances presented in the rest of this section it may be useful to bear in mind that fracture impedances of about 1 GPa s/m^3 are considered desirable. For example, in the deeper and hotter Phase II reservoir being completed now, such a low value of impedance could actually result in "self-pumping" of the reservoir because of buoyancy effects.

A. Run Segment 2

Entrance flows from EE-1 and exit flows into GT-2B during this run segment were distributed as shown in Tables IV and V. Since impedance is defined in terms of the exit flow, it is possible to assign flow impedances to each of the exit regions, as shown in Table VI. Although numerous small, sudden flow changes (the largest was 0.00126 m^3/s or 20 gpm) were observed during the test, the overall impedance decreased steadily from 1.7 GPa s/m^3 (16 psi/gpm) to 0.326 GPa s/m^3 (2.98 psi/gpm) during the 75-day flow test, as shown in Fig. 17. This large change is probably due to the extensive cooling of the entire fracture system, with consequent decrease of the fracture-closure stress and partial opening of the fractures.

TABLE IV

POSITION AND MAGNITUDE OF RELATIVE EE-1 INJECTION FLOWS, RUN SEGMENT 2

Cable Depth Interval (m)	Cable Depth Interval (ft)		Flow Fraction
2073-2179	6800-7150		0.05
2271-2377	7450-7800		0.06
2484-2530	8150-8300		0.01
2606-2652	8550-8700		0.01
2652-2896	8700-9500		0.81
2896-2957	9500-9700		0.05
		Total	1.00

TABLE V

POSITION AND MAGNITUDE OF GT-2B EXIT FLOWS, RUN SEGMENT 2

GT-2 Laboratory Cable Depth (m)	(ft)	Flow Fraction	Absolute Flow (gpm)	(m^3/s)
2660-2661	8726-8729	0.38	92	0.0058
2671-2672	8764-8765	0.05	12	0.00075
2686-2688	8812-8820	0.20	48	0.00303
2705-2706	8876-8879	0.12	29	0.00183
2719	8920	0.25	61	0.00385
	Total	1.00	242	0.0153

TABLE VI

IMPEDANCES, RUN SEGMENT 2

Fracture Depth GT-2B		Flow Impedance GPa s/m^3 (psi/gpm)			
		Jan. 30, 1978		April 12, 1978	
(m)	(ft)	Main	Secondary	Main	Secondary
2640	8660				12.6 (115)
2660	8728			0.82 (7.5)	
2670	8760			6.6 (60)	
2677	8784				54.1 (495)
2688	8820	2.2 (20)		1.67 (15.3)	
2703	8867				108.2 (990)
2707	8882			2.78 (25.4)	
2719	8920				29.5 (270)
2720	8925	8.7 (80)		1.36 (12.4)	
Fracture set		1.7 (16)		0.34 (3.12)	7.1 (65)
Entire System		1.7 (16)		0.326 (2.98)	

B. Run Segment 3 (High Back-Pressure Experiment)

The reservoir configuration during this test was the same as in Run Segment 2. However, the GT-2B pressure was raised by valve throttling to 9.65 MPa (1400 psi) in order to observe the effect of the increased back pressure on heat extraction and flow impedance. As expected, a marked decrease in flow impedance was observed, as seen in Fig. 18, and the impedance decreased during the run as the fracture was further cooled and pressurized. The pressurization of GT-2B changed the impedance from 0.82 GPa s/m^3 (7.5 psi/gpm) to 0.22 GPa s/m^3 (2 psi/gpm), based on a low back-pressure measurement made just before the high back-pressure test. A further decrease by a factor of 4 during the high back-pressure run may be attributed to increased pressurization and cooling.

C. Run Segment 4 (After Recementing and Reservoir Enlargement)

This run segment was made with a larger heat-extraction system, after the leaky annulus behind the EE-1 casing had been recemented. The major entrance point in EE-1 was moved from 2760-m (9050-ft) to 2940-m (9650-ft) depth, about 100 m below the exit region in GT-2B.

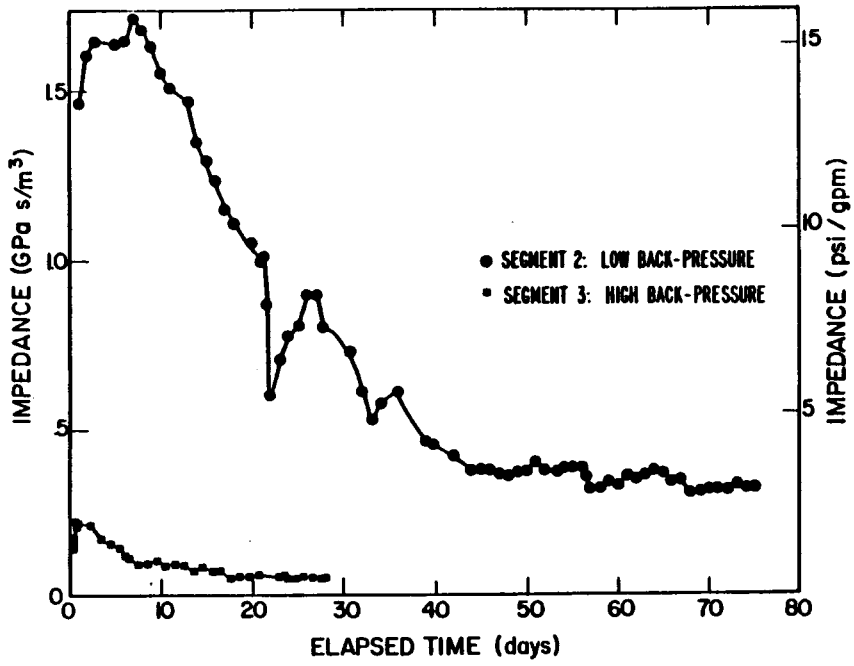

Fig. 17.
Flow impedance behavior for Run Segments 2 and 3.

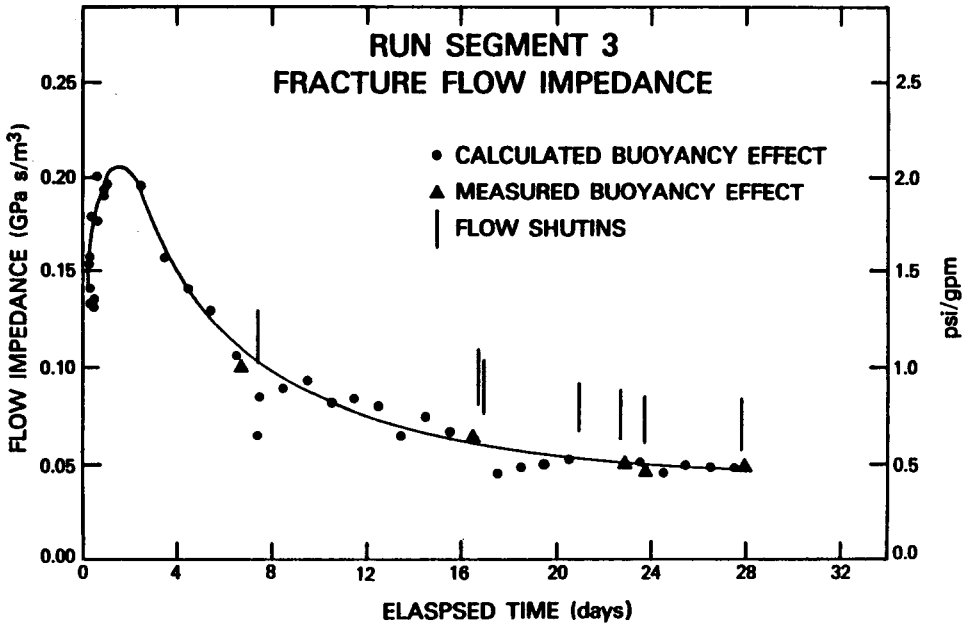

Fig. 18.
Flow impedance behavior for Run Segment 3.

Flow impedance during the run is shown in Fig. 19. Stages 1, 1A, and 2, as shown on the figure, represent transient conditions in the reservoir. The impedance at the end of stage two, during which low back pressure prevailed, approached a steady-state value near 2 GPa s/m^3 (18 psi/gpm). Note that this value is nearly identical to the initial value (before prolonged thermal contraction) observed in Run Segment 2, which was also conducted at low back pressure. Thus it can be concluded that the reservoir enlargement did not significantly increase impedance.

A short high back-pressure run was conducted as stage three. The impedance dropped by a factor greater than 2 when the GT-2B pressure was raised, to ∿0.80 GPa s/m^3 (7.3 psi/gpm), and subsequently recovered to a steady-state value of 1.85 GPa s/m^3 (17 psi/gpm) after the back pressure was reduced. This impedance remained remarkably constant during the rest of Run Segment 4. This may be attributed to the relatively small amount of cooling over the fracture face during this test, together with the constant pressure conditions.

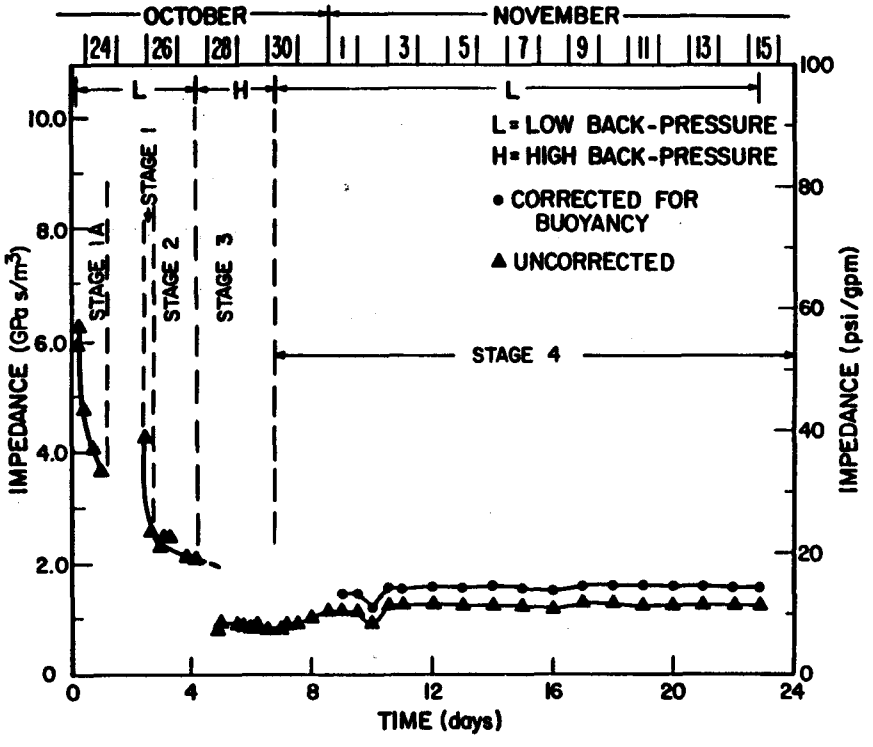

Fig. 19.
Flow impedance behavior for Run Segment 4.

D. Run Segment 5 (286-day flow test)

After an initial transient decline, the impedance during this run segment remained essentially constant at 1.69 GPa s/m^3 (15.5 psi/gpm), as shown in Fig. 20. Despite the evidence for area and volume growth cited earlier, no evidence of impedance change due to cooling of the rock was observed. In an extension of the Muskat technique for evaluation of shut-in's, a method was developed for determining the entrance, exit, and fracture impedances from shut-in data alone, without the necessity for buoyancy calculations.[5] The mean impedance values for seven shut-ins, calculated by this method, were as follows:

(a)	Entrance impedance	0.13 ± 0.03 GPa s/m^3	(1.2 psi/gpm)
(b)	Main fracture impedance	0.29 ± 0.03 GPa s/m^3	(2.7 psi/gpm)
(c)	Exit impedance	1.14 ± 0.05 GPa s/m^3	(10.4 psi/gpm)
(d)	Total impedance	1.56 ± 0.05 GPa s/m^3	(14.3 psi/gpm)

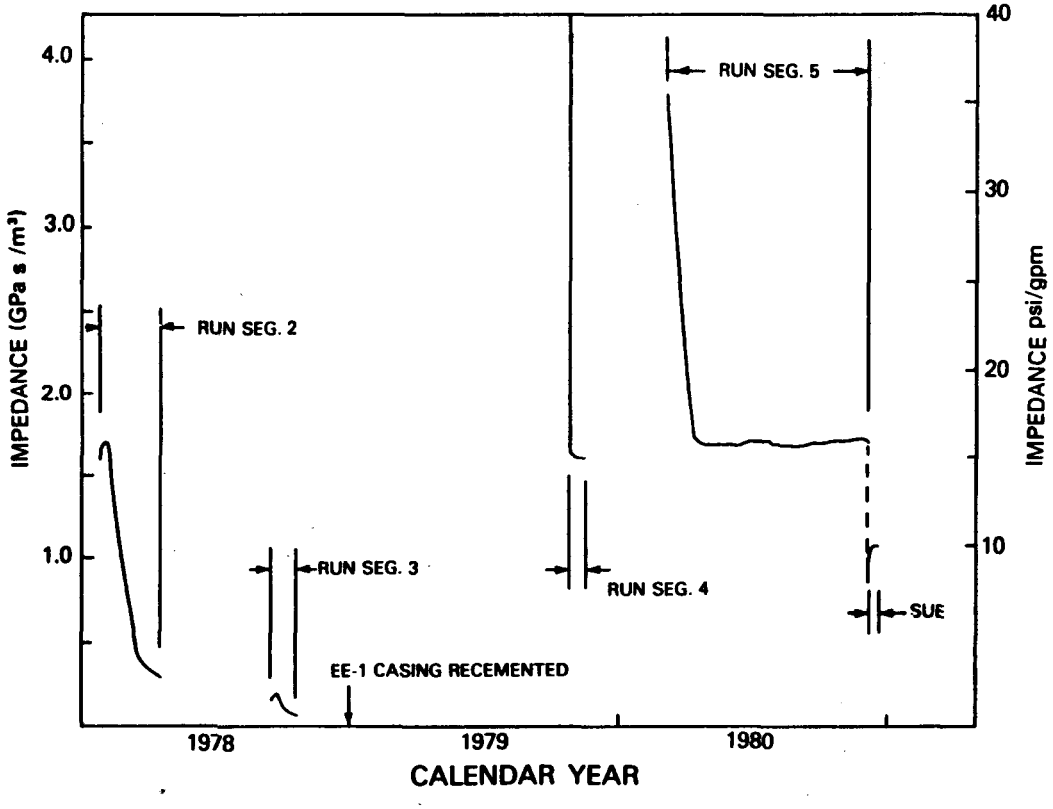

Fig. 20.
Flow–impedance behavior in the Phase I reservoirs during run Segments 2 through 5.

E. Stress Unlocking Experiment (SUE)

At the end of Run Segment 5, GT-2 was shut-in and the entire system pressurized to approximately 15 MPa in order to facilitate readjustment of the reservoir rocks to the new system of stresses, which had been generated by cooling the reservoir. Numerous microseismic signals were observed,[8] indicating that such readjustment was taking place, and changes in fracture impedance were seen in subsequent flow and shut-in experiments as follows:

(a)	Entrance impedance	0.06 GPa s/m^3	(0.55 psi/gpm)
(b)	Main fracture impedance	0.34 GPa s/m^3	(3.1 psi/gpm)
(c)	Exit impedance	0.50 GPa s/m^3	(4.6 psi/gpm)
(d)	Total impedance	0.90 GPa s/m^3	(8.2 psi/gpm)

The changes in entrance and exit impedance are statistically significant, and the main effect of SUE is seen to be a reduction of the exit impedance by a factor of two. The system was not operated after SUE for a time long enough to show that this reduction was permanent.

F. Analysis

Figure 20 summarized the impedance history over Segments 2 through 5 and the SUE experiment. Impedance is dependent on fracture aperture, w. Theoretically, it decreases as $1/w^3$ in both laminar and turbulent flow. Aperture may be increased in several ways: (1) by pressurization of the fracture, (2) cooling of the surrounding rock, (3) dissolution of minerals lining the crack by chemical treatment of the fluid, and (4) by geometric changes resulting from relative displacement of one fracture face with respect to the other. Run Segments 2 and 3 were especially useful in demonstrating the correlation between impedance and pressure and temperature, as may be seen in Figs. 21 and 22. The impedance changes observed after SUE were probably due to additional "self-propping" caused by slippage along the fracture faces near the exit or by other pressure-induced geometric changes.

The concentration of impedance near the exit, shown in all the low back-pressure flow experiments, may be desirable when the system impedance is reduced by multiple fractures. In this mode of reservoir development, the possibility of unstable "runaway" (one fracture cooling and taking much of the flow) exists, and the exit impedance concentration will prevent this until reservoir cooling has been extensive. Eventually, the problem of flow control in the individual fractures may arise, and methods of flow control near the fracture entrance may be required.

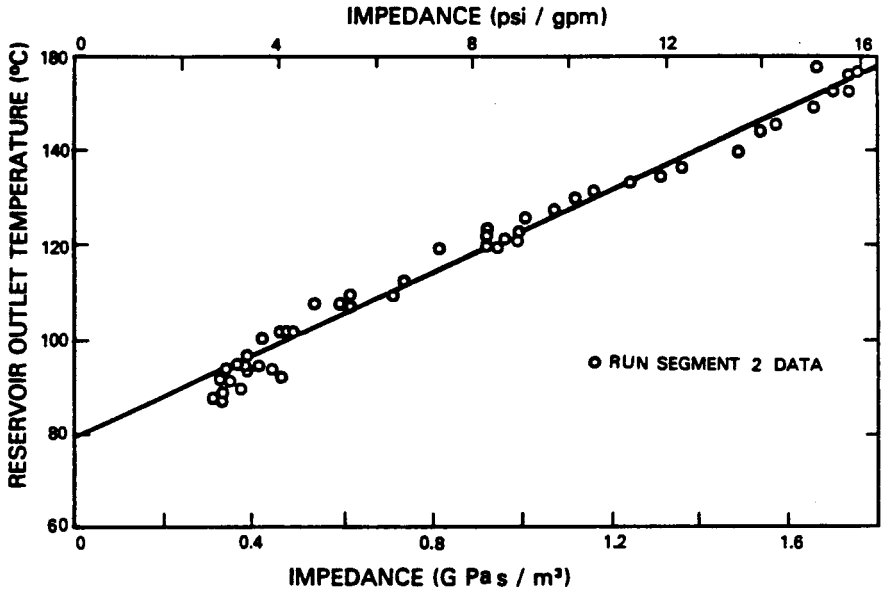

Fig. 21.
Fracture system specific flow impedance vs reservoir outlet temperature, Run Segment 2.

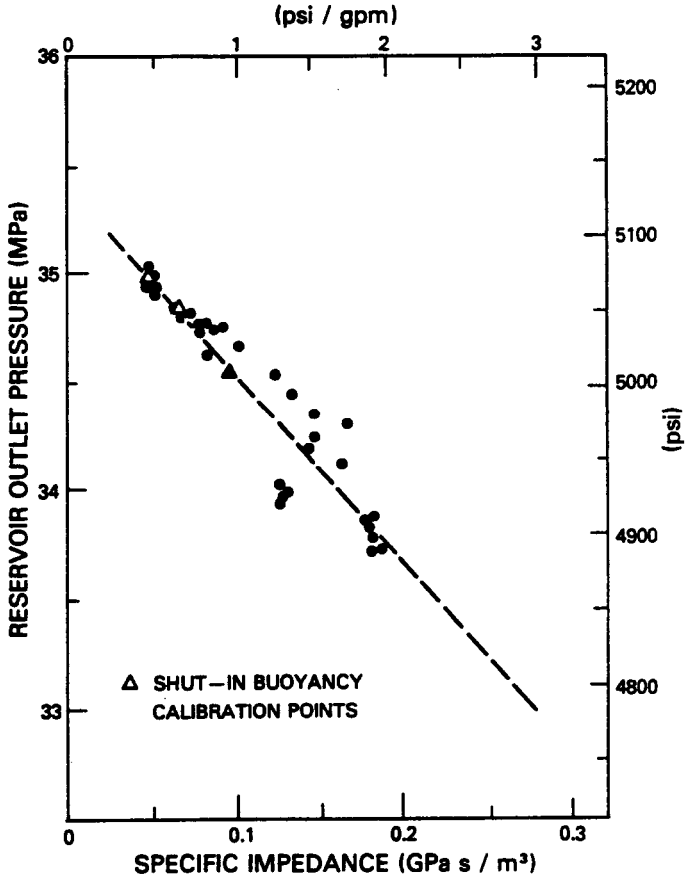

Fig. 22.
Fracture system specific flow impedance vs reservoir outlet pressure, Run Segment 3.

During normal, low back-pressure conditions* fracture impedance appears to be concentrated near the exit well, at least after a short period of operation, and total impedance does not depend strongly on wellbore separation. Impedances are sufficiently low to allow operation of efficient HDR geothermal energy-extraction systems. The impedance in a large system does not change rapidly, and the prognosis for operation of the multiple-fracture, Phase II system seems favorable.

VI. WATER LOSSES

The water loss of an HDR system is very important because this water must be provided from some outside source. This information can be vital for environmental as well as economic reasons. The water-loss rate, that is, the rate at which water permeates the rock formation surrounding the fracture system, is the difference between the injection rate and the produced, or recovered, rate at GT-2B. This loss rate is a strong function of system pressures and flow rate and would also be expected to be a function of reservoir size.

The water-loss flow-rate data of each experiment contain many transients due to operational shutdowns, pump limitations, and various leaks. Consequently, the accumulative volume of water loss is best suited for comparisons since many of the transients are smoothed out, and this comparison is presented in Fig. 23, for Run Segments 2, 3, and 5. Run Segment 4, only 23 days long, was excluded from this comparison because of the disparate conditions under which it was conducted -- four separate stages of wellhead pressure conditions were imposed. The first stage actually consisted of hydraulic fracturing, so the water losses were expectedly high. The succeeding stages consisted of alternating sequences of high, then low back pressure, so that comparison with the other run segments, in which pressure conditions were far less variable, is impractical.

Referring back to Fig. 23, comparisons between Run Segments 2 and 5, both conducted under normal, low back-pressure conditions, can be made as follows. Direct comparisons indicate that the water loss for Run Segment 5 is approximately 40% higher than that of Run Segment 2 at comparable times after the

---

*For operational purposes, for example, design and operation of surface piping, heat exchangers, etc., we normally prefer the low back-pressure mode of operation.

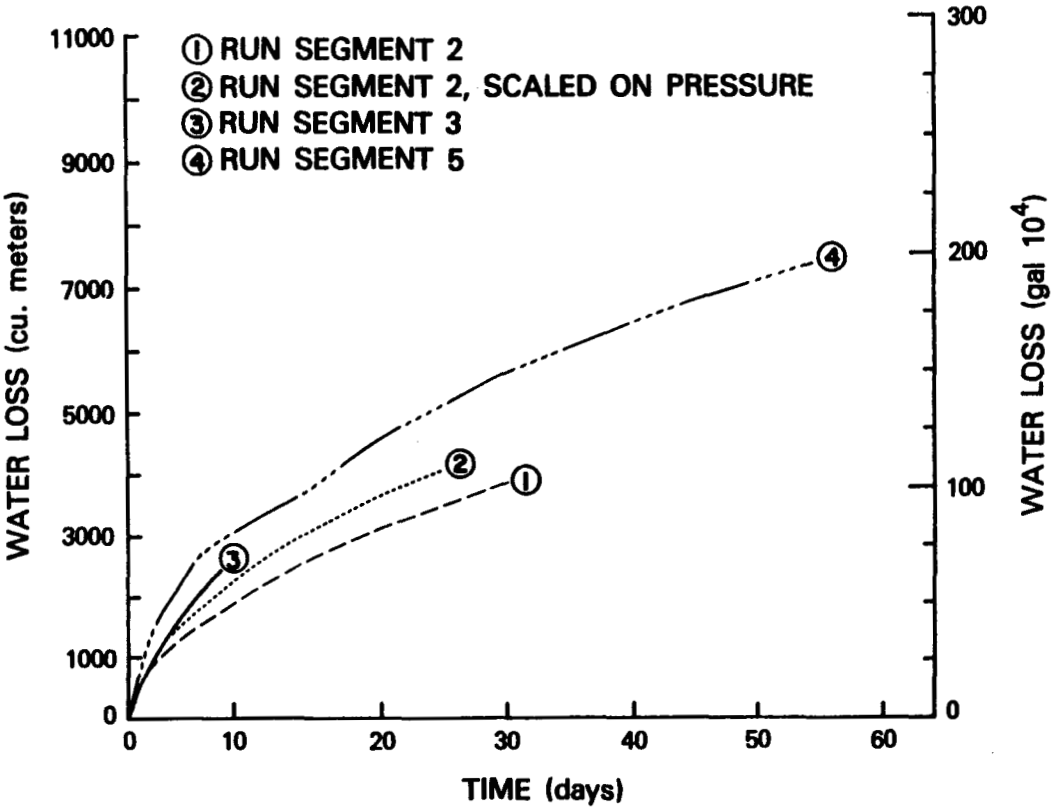

Fig. 23.
Cumulative water losses vs time for Run Segments 2, 3, and 5.

beginning of heat extraction. However, because the operating pressure was 10% higher during Run Segment 5, the water loss for Run Segment 2 should be scaled up by 10% as in curve 2 of the figure, in order to be directly comparable to Run Segment 5. Then it is seen that the Run Segment 5 water loss is only 30% higher than Run Segment 2, despite a several-fold increase in heat-transfer area and volume. An obvious conclusion is that the heat-exchange system utilizes only a small portion of a much larger fracture system that controls water loss. This large, potential fracture system was not altered to any large extent by the MHF experiments of Segment 4. In fact, this was seen near the conclusion of the heat-transfer section, where it was noted that the heat-transfer area was small compared with the other areas indicated by seismic, inflation, or venting measurements. Furthermore, in comparison to the heat-transfer areas, these other areas did not grow significantly from Run Segments 2 through 5.

At the end of Run Segment 2 the actual water loss rate was only 1×10^{-4} m^3/s, about 1% of the total flow rate circulated through the reservoir. However, this extremely low loss rate was due to the gradual decrease in surface pressure after 30 days. The loss rate extrapolated to the end of the experiment and by model fits to the first 30 days is 7×10^{-4} m^3/s (7%). At the end of Run Segment 5 the loss rate was 6×10^{-4} m^3/s, about 10% of the circulated flow rate. The Run Segment 3 losses are slightly larger than those of Segment 2, which is consistent with the fact that both EE-1 and GT-2B were pressured in Run Segment 3. At the end of Run Segment 3 the loss rate was 1.3×10^{-3} m^3/s, about 14% of the circulating rate.

The use of a pressure-dependent, water-loss diffusion model[2,5,20] confirms these comparisons. The theoretical fits to the data are most sensitive to two parameters: (a) $\alpha = A\sqrt{k\beta}$, which is evaluated at starting or hydrostatic pressure (where A is the diffusion area, k the permeability, and β the system compressibility) and (b) C, a constant that determines the pressure dependence of α (see Ref. 20). This parameter is best interpreted as the reciprocal of the sum of the confining stress and a fracture modulus. Values of α and C, obtained from numerical modeling, are tabulated in Table VII.

Similar to the water losses, the α for Run Segment 5 is ~30% higher than that of Run Segment 2 and probably reflects the addition of the lower half of the reservoir. The value of C was determined mainly by one flow transient in Run Segment 5. The range of C^{-1} indicated in the table reflects the lack of sensitivity to this parameter. Short-term transients, even in the water losses, measure some local parameters. It is possible that the response of the lower half of the reservoir is determined by a larger component of <u>in situ</u> stress.

TABLE VII

WATER LOSS DIFFUSION PARAMETERS

Run Segment	α ($m^3 MPa^{-1/2}$)	C^{-1} (MPa)
2	1.4×10^{-6}	9.3
3	1.4×10^{-6} to 2.8×10^{-6}	9.3
5	1.9×10^{-6}	$13.3 \lesssim C^{-1} < 20.0$

VII. FLUID GEOCHEMISTRY

Analysis of the fluid-chemistry data from the Phase I reservoirs shows several interesting features that are pertinent to the size of the reservoirs. Strong evidence from each of the Phase I heat-extraction experiments indicates the existence of essentially two parallel flow paths: (1) a fracture-dominated flow path (perhaps consisting of multiple fractures) that includes the heat-transfer surfaces, and (2) a high-impedance flow path consisting of the connected microfractures and pores in the rock surrounding the heat-extraction portion of the reservoir. Displacement of the indigenous pore fluid contained in this high-impedance flow path is the single most important geochemical effect observed in the heat-extraction experiments to date.[21]

The flow rate at which the pore fluid is displaced into the circulating system has been calculated for Run Segments 4 and 5 by considering the increase in concentration of dissolved chemical species as the fluid passes through the downhole system. Similar calculations for Run Segments 2 and 3 are not conclusive as steady-state conditions were never achieved in the fluid geochemistry of these experiments. The results of the calculations of pore-fluid flow fraction are plotted in Figs. 24 and 25 for Run Segments 4 and 5, respectively. Three main assumptions were made: (1) the pore-fluid concentration is constant in time and space, (2) the residence time of the primary-fracture flow path is very small so that the pore fluid initially in this portion of the system is quickly displaced, and (3) no reactions occur that change the fluid composition as it passes through the fracture flow path. As is evident in Fig. 24, the secondary-flow fraction in the low back-pressure portion of Run Segment 4 is approximately 10% of the production flow rate while in Run Segment 5 (also at low back pressure) the fraction is roughly 5% (Fig. 25). This difference in flow fractions probably results from the difference in pressure drop across the reservoir in each of the Run Segments -- 8.5 MPa (1238 psi) in Run Segment 4 as opposed to 7.0 MPa (1020 psi) in Run Segment 5. (See Table VIII.) On the other hand, dilution of the pore fluid by fresh water in some of the secondary flow paths could be responsible for an apparent change in secondary flow fraction.

By either mechanism, the volume of undiluted pore fluid displaced into the circulating system is tremendous. During Run Segment 5, a pore-fluid flow rate of 3×10^{-3} m^3/s (4.4 gpm) -- roughly 5% of the production flow rate -- for the duration of the experiment would constitute an undiluted cumulative

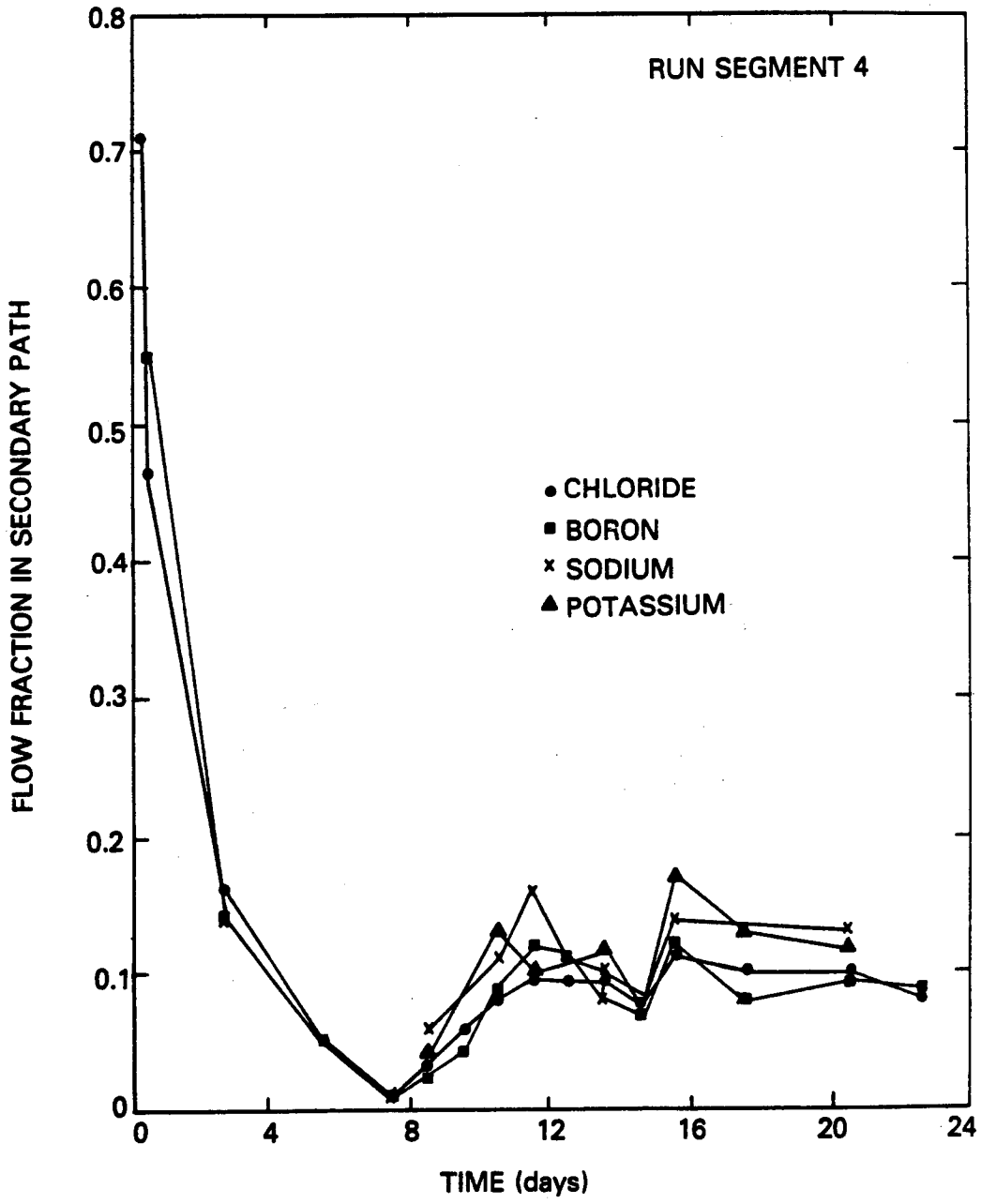

Fig. 24.
Calculated flow fraction of pore fluid from secondary flow paths from Run Segment 4.

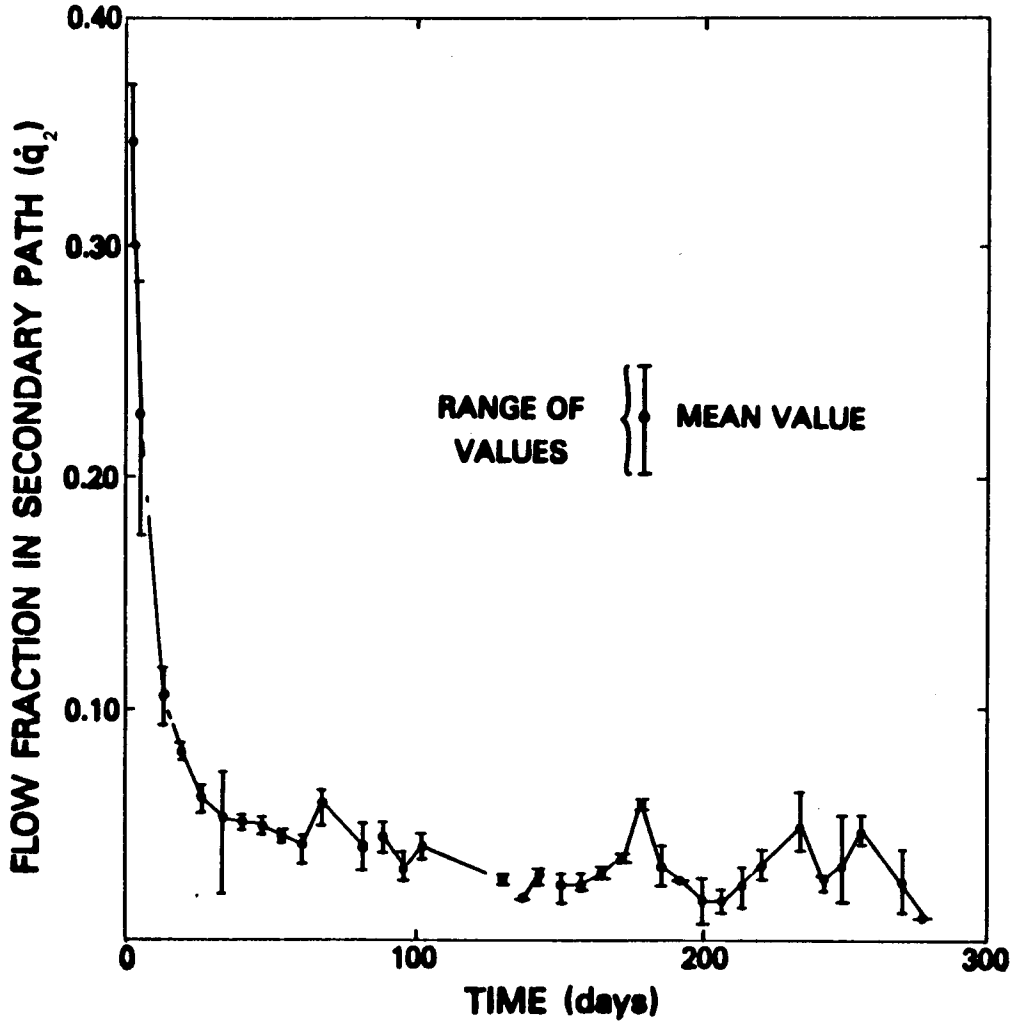

Fig. 25.
Calculated flow fraction of pore fluid from secondary flow paths from Run Segment 5.

pore-fluid volume of 6700 m^3 (1.8 x 10^6 gal). The pore-fluid displacement rate is approximately half of the steady-state water loss rate during Run Segment 5 (after correcting for the EE-1 annulus leak). Similarly, the pore-fluid displacement rate is half of the water loss rate during the steady-state, low back-pressure stage of Run Segment 4 (Table VIII).

In summary, several conclusions should be drawn from geochemistry results to date. First of all, the overall circulating fluid quality in a HDR system is largely fixed by the pore-fluid concentration and displacement rate. Under the very worst conditions (that is, 100% of the produced fluid is pore fluid) the maximum concentration of dissolved solids would be around 5000 mg/ℓ for this reservoir -- within the Environmental Protection Agency (EPA) water

TABLE VIII

SYSTEM OPERATING PARAMETERS DURING STEADY-STATE, LOW BACK-PRESSURE PORTIONS OF RUN SEGMENTS 4 AND 5.

	Run Segment 4	Run Segment 5
EE-1 injection pressure	9.7 MPa	8.3 MPa
GT-2 production pressure	1.1 MPa	1.2 MPa
EE-1 flow rate	0.0076 m^3/s	0.0057 m^3/s
GT-2 flow rate	0.0063 m^3/s	0.0052 m^3/s
Water-loss rate	0.0013 m^3/s	0.0006 m^3/s
Pore-fluid displacement rate	0.0006 m^3/s	0.0003 m^3/s

quality standard for continuous irrigation of salt-tolerant plants. However, the steady-state concentration of total dissolved solids is typically 2500 mg/ℓ -- similar to water used for human consumption in many parts of the country. The pH of the water is 6.5 ± 0.5, nearly neutral, and problems with corrosion or deposition upon surface equipment such as piping, heat exchangers, and pumps have been minimal.

A second conclusion from the fluid-geochemistry studies concerns the very large volume of pore fluid that has been displaced from the rock surrounding the fracture system <u>into</u> the fracture system. Because this fracture system is everywhere pressurized above hydrostatic pressure, circulating fluid should be continuously lost to the surrounding matrix, which is subhydrostatic. Pore-fluid from this subhydrostatic pressure field would have to flow against a pressure gradient in order to enter the flowing system. However, secondary flow paths with impedance intermediate to that of the main fracture system and that of the unfractured reservoir rock provide a means for the pressure level in the main fracture(s) to displace the pore fluid into the flow system. Models of this behavior are currently being developed.

Finally, the flow from these secondary paths appears to be partially sensitive to the pressure difference between the inlet and outlet and probably, to the overall level of pressurization of the reservoir. Massive pressurization of the reservoir (such as occurred during SUE) or alternative methods of heat-extraction operation such as "huff-puff" (see Sec. X), may unlock the

potential that exists for gaining access to these secondary flow paths and for extracting the heat from a much larger volume of rock than is currently available in the Phase I system with the usual flow-through, circulating mode of heat transfer.

VIII. SEISMICITY

Seismic monitoring was conducted for all the run segments. The objectives of this monitoring are: (1) evaluation of potential seismic risks associated with HDR geothermal energy extraction, and (2) use of microseismic events to infer reservoir geometry. Continuous monitoring was conducted with a surface seismic array, for all run segments, and during portions of Run Segments 4 and 5, and SUE, with downhole geophone packages positioned in the reservoir vicinity. The surface array consisted of six stations within 750 m (1/2 mile) of the site, five borehole stations located within 10 km of the site, and the Los Alamos National Laboratory regional net -- the nearest of which is located at 10 km. The sensitivity of this surface array extended to Richter earthquake magnitudes of 0 to -1.5 and is limited by the nearly 3 km of vertical separation and the large seismic attenuation of the near-surface sediments and volcanics. Each downhole geophone package consists of 12 geophones, 4 each in the x-, y-, and z-direction axes. Typically the sensitivity of these downhole packages extends to local magnitudes on the extrapolated Richter scale as low as -6. For both Run Segments 4 and 5 a single downhole package was positioned in EE-2, which was drilled for the Phase II reservoir, and used simply as an observation well in these experiments. During SUE an additional geophone package was positioned in the production well GT-2B.

Addressing seismic hazards first, there apparently are none. The largest event detected in Run Segment 4 with the downhole package had a magnitude of -1.5. The energy release of a -1.5 magnitude microseismic event is roughly equivalent to that of a 10 kg mass dropped 3 m. Furthermore, this event occurred during the high back-pressure stage. During the low back-pressure stage, more typical of ordinary heat-extraction conditions, the largest event was -3. During the 286-day Run Segment 5, 13 microearthquakes ranging between -1.5 and 0.5 were recorded by the surface seismic array. These events were located about 200 m north of EE-2 at a depth of about 1 km. The events are not related to Run Segment 5 activities, but rather to the drilling of EE-2 and EE-3. They began about 11 days after EE-2 began losing large amounts [as much

as 2 x 10^{-2} m^3/s (450 000 gal per day)] of drilling fluids at the lithologic boundary separating the sediments and volcanics from the Precambrian crystalline rocks below. This fluid loss was caused by a casing failure during the drilling operation. The related seismic events subsided about 60 days after the casing was repaired, but before that about 3 x 10^4 m^3 (8 000 000 gal) of fluid were pumped into the unconformity. It is believed this fluid triggered the release of tectonic stress in that portion of the basement adjacent to the unconformity. The cumulative seismic-energy release of these events was about that of a magnitude 0.75 earthquake. We reiterate that even these small events are related to drilling, not reservoir operations.

We turn now to the other task, which is to use microseismic event locations to predict in a quantitative fashion the geometry of the resulting 3-dimensional temperature field with time as heat is extracted. Discussions with electric utility representatives have made clear the fact that commercial use of future reservoirs requires firm estimates of expected useful lifetime. Up to now our firmest estimates are based upon modeling of thermal drawdown, which requires long and expensive testing. Only through the experience gained from numerous past experiments can this testing period be bypassed. Recourse to measured thermal drawdown in the recovery well of a large reservoir with a calculated useful lifetime of 10 or more years would add an overwhelming financial burden.

An examination of the various methods we have employed to measure and characterize these systems reveals only two at this time with the potential of providing this needed information. The first of these, discussed earlier, involves measurement of fracture volumes with tracers and correlating volumes with heat-exchange areas. The second method is microseismic mapping, which is discussed in the remainder of this section.

Past observations of the microseismic response associated with the creation and operation of our HDR reservoirs lead to the following conclusions:

1. Microseismic activity is always present during initial fracturing.
2. There exists a pressure threshold for microseismic activity; above this threshold pressure, related to the minimum earth stress, significant microseismic activity can be generated.
3. The events observed during the initial stage of pressurization are in general clustered about a vertical plane whose strike has

remained remarkably constant. We will refer to this as the planar-event region.

4. Continued pressurization and water-loss diffusion results in a general displacement of microseismic events to considerable distances ($\geq$500 m) away from both the injection point and the planar locus of events. This will be referred to as the nonplanar-event region.
5. The location of the zone of heat removal occupies a portion of the planar-event region.
6. The surrounding volume of rock space defined by the nonplanar seismic events is not an important part of the active HDR system with the present wellbore geometry.
7. There is only very low-level seismic activity associated with the active heat-exchange regions of the Phase I reservoir. Apparently thermal depletion, accompanied by rock shrinkage, has rendered these regions aseismic.
8. Pressurization of the partially drawndown reservoir during SUE resulted in significant seismic activity starting at pressures lower than those observed with pressurization of uncooled systems. This thermal stress/pressurization augmentation of microseismicity appears to originate in regions just outside and peripheral to the active heat-exchange regions.

The vertical dimension of the planar-event region that bounds the aseismic zone and that extends from ~2820 to 2950 m, coincides quite closely with the location of the region of significant thermal drawdown determined from the latest EE-1 thermal-recovery survey shown in Fig. 26. Figure 27 shows plan and elevation maps of the hypocenters of the SUE events displaying the more likely of two sets of solutions. Reference 8 provides analysis of the location methods applied to the information obtained from both geophone stations operated during the experiment. Of particular interest is the aseismic region centered about the EE-1 well-to-reservoir injection location. Its location and general size (diameter ~100 m) are suggestive of an area that may be attributed, for Run Segment 5, to the cooled region centered about the cold-water injection location. Assume now that the severe thermal contraction resulting from heat-extraction stress relieves the rock to such an extent that subsequent pressurization produces no further failure. The separation of the SUE microseismic-event sequence into 1-h intervals, as shown in Figs. 28 to

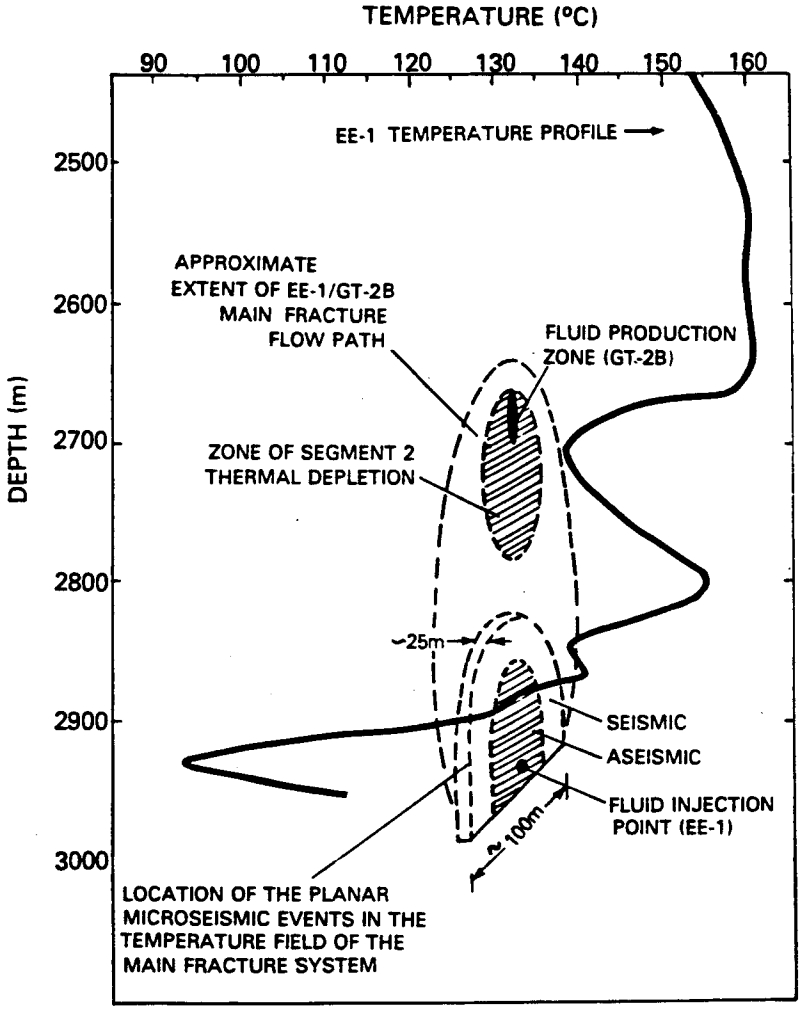

Fig. 26.
Recovery temperature survey in EE-1 (7/10/81) showing correlation of the region of thermal drawdown with the planar-event and aseismic regions.

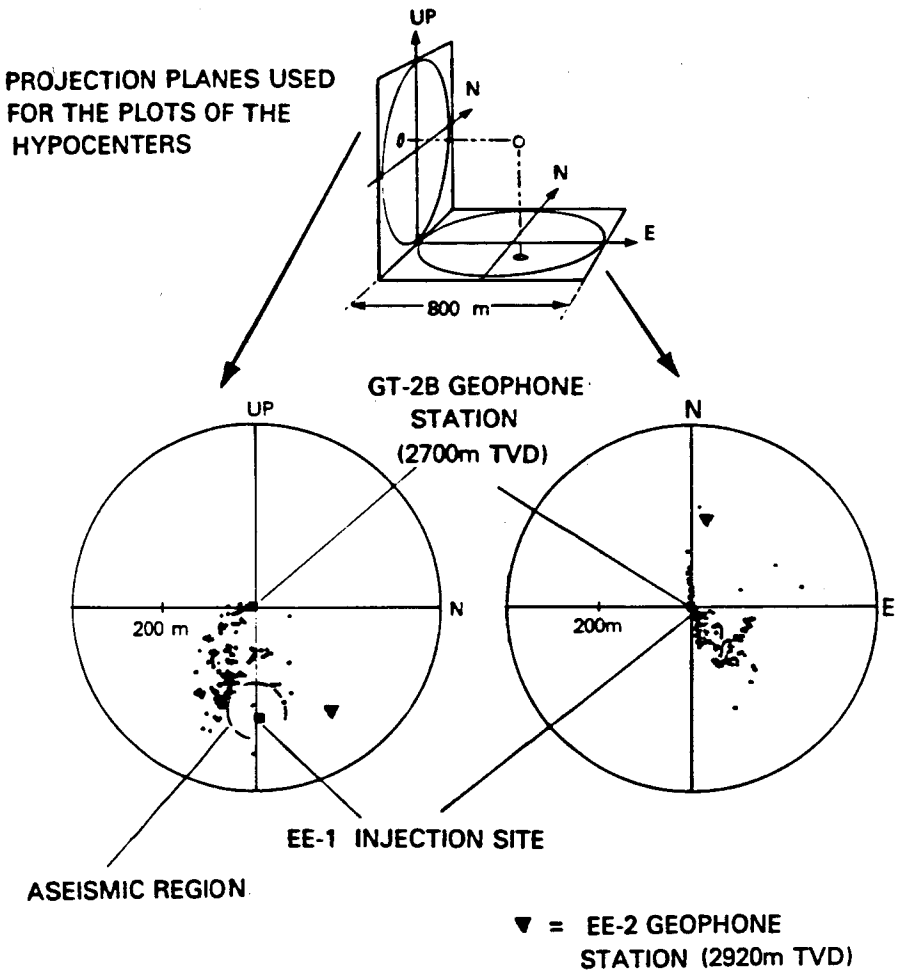

Fig. 27.
Elevation view (left) and plan view (right) of microseismic events located by the two-station method during SUE. The aseismic region around the EE-1 injection site is seen on the north-south plane (elevation view).

30, allows further examination of this hypothesis. The upper figures labeled 16:42-17:44 on Fig. 28 show the events during the first hour of pressurization. In the plan view (Fig. 28 upper right) the grouping of the events occurs in a rather narrow, linear fashion. The trend or strike of this group in a slightly west of north direction is consistent with that obtained from earlier experiments. Of still greater interest is the grouping of events in a narrow band just outside of the boundary of the aseismic region as can be seen in the elevation view (Fig. 28 upper left). These events, which occur over a ~150-m-depth interval, must lie in a near-vertical planar zone whose extension passes quite close to the reservoir injection and recovery sites.

The next time sequence (Fig. 28, 17:48-18:50) shows a growth in the lateral extent of the linear event group. Also apparent is the appearance of a cluster of events separated from the main group. The elevation view (lower left) again locates those events that were in the linear group in the same narrow band (plan view, lower right). The cluster of events is located adjacent to the band but outside of the planar feature. One might assume that this is activity associated with the expanding pressure field moving out away from the heat-transfer system. The next time interval (Fig. 29, 18:56-19:37) continues the sequence. The off-plane group activity has moved upwards as has some of the planar activity. The fourth sequence (Fig. 29, 19:59-21:00) has the planar activity dying away, along with the appearance of a new cluster group lying higher and further away. The plan view (lower right) of these several regions suggests their parallel nature. The fifth sequence (Fig. 30, 21:02-22:04) is more difficult to explain in that a fewer number of events occurred and the second cluster is missing. The final sequence (Fig. 30, 22:09-23:10) still shows activity in the zone adjacent to the aseismic zone and also the reappearance of the second cluster.

It is interesting to consider whether stress relieving of the aseismic zone due to extensive cooling has increased the stresses in the surrounding region. Such stresses could be released by a pressure wave moving outwards from the injection point, through the aseismic zone and then into the stressed region.

If this interpretation of the seismic history of SUE is indeed correct, it holds great promise as a means of following both the extent and location of the portion of a HDR reservoir from which thermal energy is being extracted. Periodically the system would be shut-in while continuing flow into the

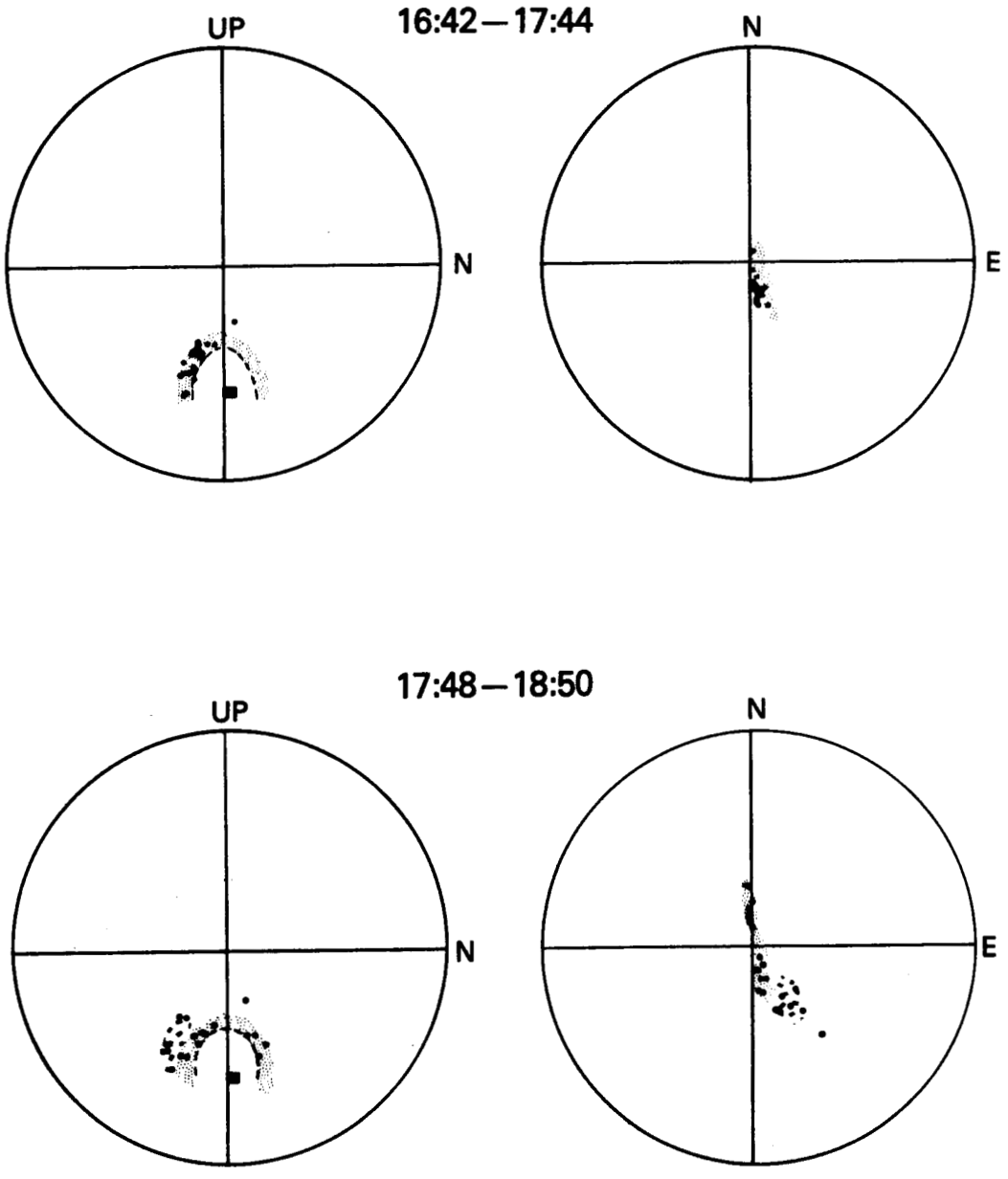

Fig. 28.
Elevation view (left) and plan view (right) maps of microseismic activity during the first and second 1-h intervals of SUE (December 9, 1980).

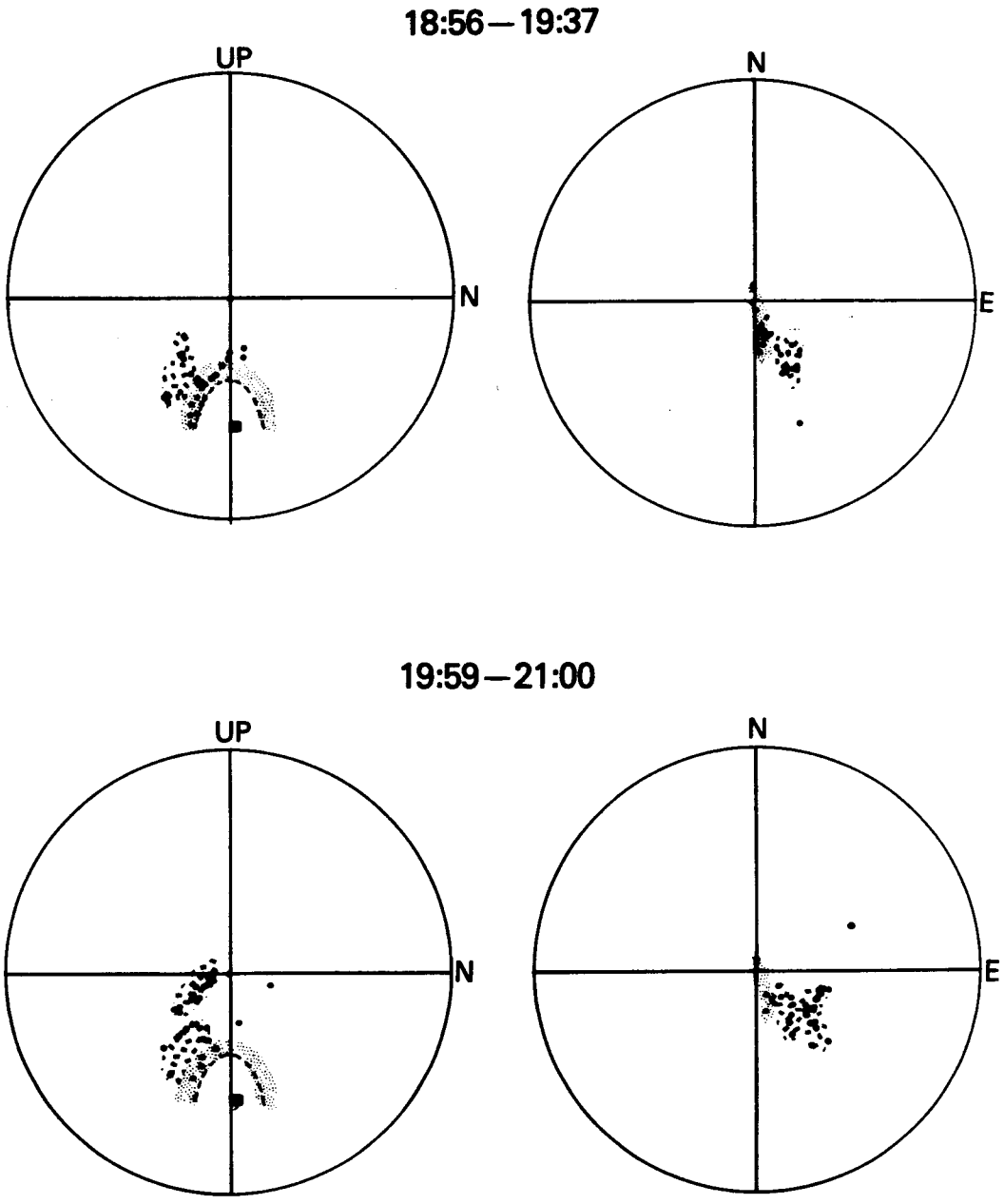

Fig. 29.
Elevation view (left) and plan view (right) maps of microseismic activity during the third and fourth 1-h intervals of SUE (December 9, 1980).

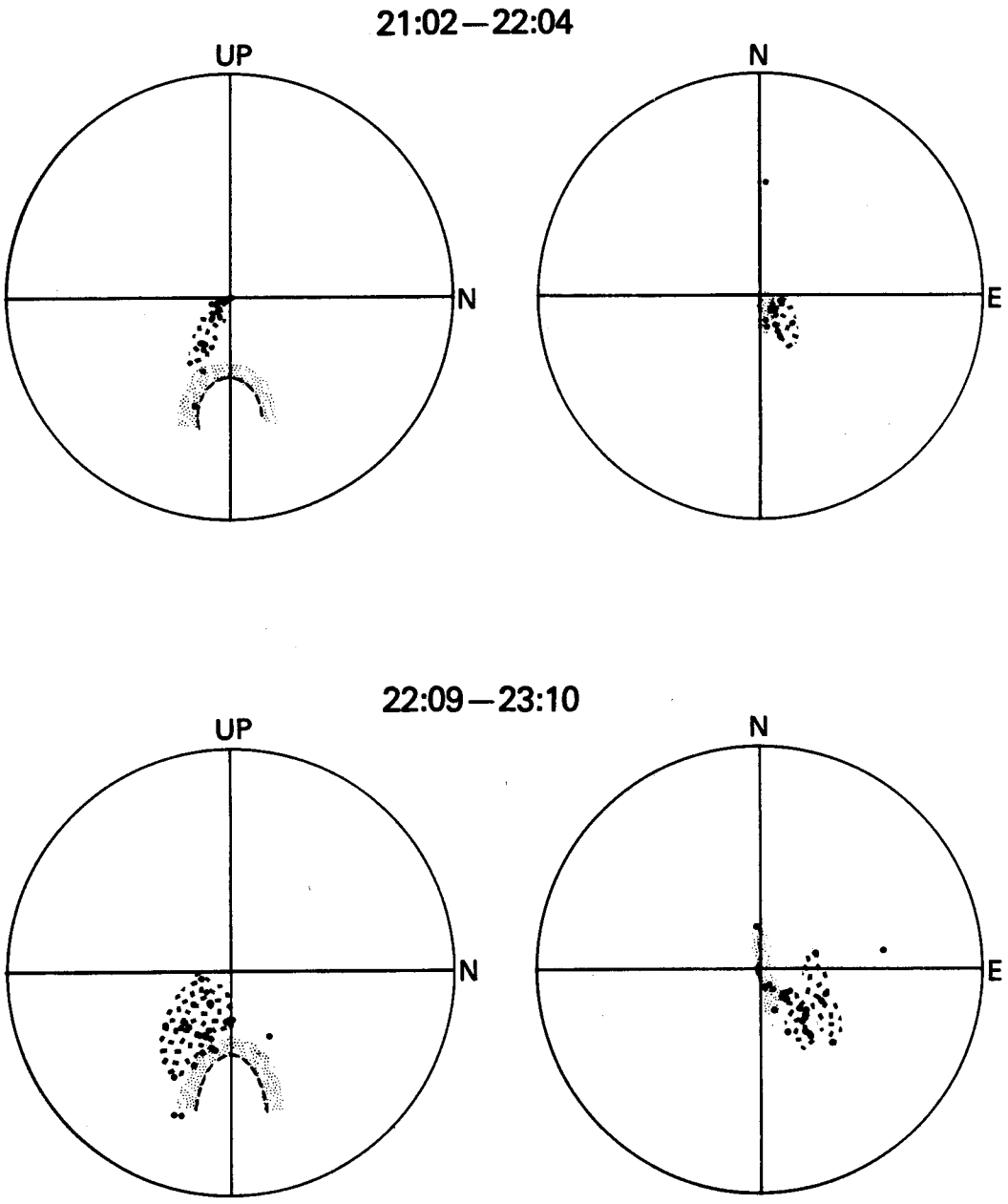

Fig. 30.
Elevation view (left) and plan view (right) maps of microseismic activity during the fifth and sixth 1-h intervals of SUE (December 9, 1980).

system. If the SUE experiment is repeatable, there would be very early mappable seismic activity bordering the severely drawndown region. If this composite region, composed of the aseismic zone and the adjacent band of microseismic activity, with its known geometry, continues to correlate with the heat-transfer area derived from temperature recovery surveys in EE-1, then its identification by microseismic mapping techniques may provide the long sought predictive tool needed in HDR reservoir engineering.

IX. CONCLUSIONS

The reservoirs of the Phase I HDR geothermal energy system have exhibited growth through all segments of operation. This growth resulted from pressurization, cooling (thermal contraction), and fracture-face displacement or movement. During the early time experiments (Run Segments 2 and 3) thermal drawdown was significant due to the small size of the reservoir involved (90°C for Segment 2 and 37°C for Segment 3). In the later experiments, drawdown was much less significant due to the larger reservoir. No drawdown was observed during Segment 4, and during Segment 5 operations, the reservoir sustained only an 8°C thermal drawdown after 286 days. Modeling of the Phase I reservoirs led to an estimated heat-transfer area of 8000 m^2 for Run Segment 2, while by the end of Run Segment 5 the heat-transfer area was estimated to be 45 000 to 50 000 m^2, about six times larger. Measured tracer volumes suggested a fracture area of 80 000 m^2 by the end of Segment 5. Modal volume of the reservoir has grown from 11 to 266 m^3 through the course of Phase I experiments.

Water losses were very encouraging because, for comparable operating pressure conditions, only a 30% increase of water loss was observed for a sixfold increase in heat-transfer area. The impedance remained constant throughout Run Segment 5 at about 1.6 GPa s/m^3. This is in contrast with the Run Segment 2 reservoir that exhibited a sharp decline in the impedance, presumably due to the large thermal drawdown that the system experienced. If an impedance similar to that experienced during Run Segment 5 occurs in the Phase II reservoir under development, the system could essentially be self-pumping.

Geochemical monitoring of the system provided valuable insight concerning pore-fluid displacement and flow connections in the reservoir. The concentrations of dissolved chemicals in the produced water were relatively low and the pH was near neutral, so the produced water was of good quality and problems

with corrosion or scaling of surface equipment have been minimal. Seismic activity in the Phase I reservoirs has been insignificant. Events associated with heat extraction have measured less than minus one on the extrapolated Richter scale.

X. RECOMMENDATIONS

Based upon three years' experience with the Phase I reservoir, summarized above, we offer three recommendations: the first of these, a rather broad one, is for future experiments involving new methods of extracting heat from the reservoir; a second recommendation concerns improved microseismic mapping; and a third recommendation is for a new geochemistry experiment to better define the role of the secondary flow paths in the reservoir.

A. Improved Methods of Heat Extraction

The summary of heat extraction tests in Run Segments 2 through 5 presented in this report indicates that the Phase I reservoirs created to date are of modest size, representing about 50 000 m^2 of effective heat-transfer area. However, other indications such as geochemical, microseismic, water losses, and venting volume measurements suggest that the reservoir is potentially much larger. In particular, the microseismic data suggest that we have forced water, that is, gained access to distances very far from the injection well. Roughly speaking, a circle drawn around the microseismic epicenters measured during Run Segment 4 has an area of about 500 000 m^2, about 10 times the effective heat-transfer area. For three fractures, per the multiple-fractures model, Table II suggests a microseismic area of 360 000 m^2. Furthermore, the microseismic data suggest that this larger potential reservoir is not planar, but highly jointed and multiply fractured, so that the potential reservoir, if sufficiently exploited, would represent a volumetric rather than an areal source of heat. For the same level of power production a volumetric source results in less thermal decline than an areal source, which is severely limited by the requirement to conduct heat in the low-conductivity rock for large distances perpendicular to the areal plane.

The explanation for the large difference in reservoir sizes provided by heat-transfer results and the other indications, such as geochemistry and microseismicity, etc. is provided by fluid mechanics and flow patterns in reservoirs. Even if a reservoir was physically large, should fluid-dynamic short circuiting occur, then the effective heat-transfer size of the reservoir would

be much smaller. The most important criterion is the separation between reservoir inlet and outlet. For continuous flow circulation, in what we refer to as the low-buoyancy mode of heat extraction, it can be shown that, roughly speaking, the effective heat-transfer size is proportional to the square of the inlet-to-outlet spacing for singly fractured reservoirs and proportional to the cube of the separation for volumetric, multiply fractured reservoirs. As discussed below, these guidelines must be modified when buoyancy or natural convection effects are present, or for the cyclic (huff-puff) mode of heat extraction, also discussed below. However, for the typical conditions prevailing during Run Segments 2 through 5 these conditions did not prevail, so the general principle that separation distance controls heat extraction was in effect. In the first reservoir, before recementing and enlargement, the separation was of the order of 100 m and it is not surprising that the heat-transfer area was initially only 8000 m^2. In the second reservoir the separation is 300 m and the effective area is 50 000 m^2 when the observed thermal decline is interpreted with the independent-fractures model. Using the newer multiple-fracture model, we estimate an area of about 45 000 m^2, in reasonable agreement with the first estimate. In either case the fluid dynamics dominated, so that the heat production was limited by the separation of inlet and outlet.

In connection with this conclusion regarding fluid-dynamic limitations to heat production, it must be pointed out that the design of the Phase II reservoir, currently under construction at Fenton Hill, is based largely upon Phase I technology and experience. Of particular importance is the fact that the vertical spacing of the Phase II wellbores is 370 m, only 20% larger than that of Phase I. Consequently, we believe that heat production in the Phase II fracture will be subject to the same fluid-dynamic limitations.

There exist two general means of attacking this problem:

(1) Deviate (sidetrack) one or both of the wells so that the distance between the reservoir inlet and outlet can be increased. In this manner the new fluid streamlines would sweep over those regions of the reservoir inaccessible with the old fluid circulation patterns. This is an expensive method, and we will not consider it further here in view of funding limitations.

(2) Improve the fluid streamline patterns, without redrilling, by changing the mode of heat transfer. One means of doing so is to resort to cyclic (huff-puff) operation, in which water is injected while the production well is

shut-in. If the pressure and flow-rate conditions are appropriate, water can be forced to the reservoir extremities, and in so doing will be heated. The heated water is then withdrawn by venting the production well in the "puff" phase of the cycle. A corollary effect of cyclic operation is due to the higher pressures associated with cyclic operation -- there is the possibility (see Fig. 13) that the reservoir will grow continuously.

A second means of improving the flow streamline pattern is to promote the effects of high buoyancy.[14] This high buoyancy effect is depicted in Figs. 31 and 32. In these figures we are examining computed results for a vertically oriented, circular fracture in which the inlet and outlet locations are separated by 400 m, nearly the same value as the Phase II reservoir separation. The fracture is 0.5 km in radius. In these figures, because of symmetry, only the right-hand half of the fracture is shown. In the first figure the flow impedance is so high that buoyant, or natural convection, effects are entirely suppressed. The streamlines flow directly from inlet to outlet and bypass

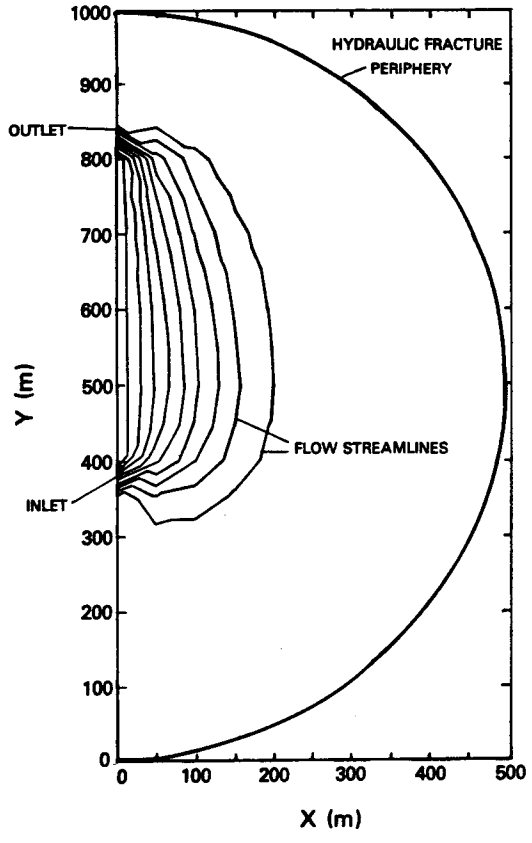

Fig. 31.
Flow streamlines with negligible buoyancy contribution.

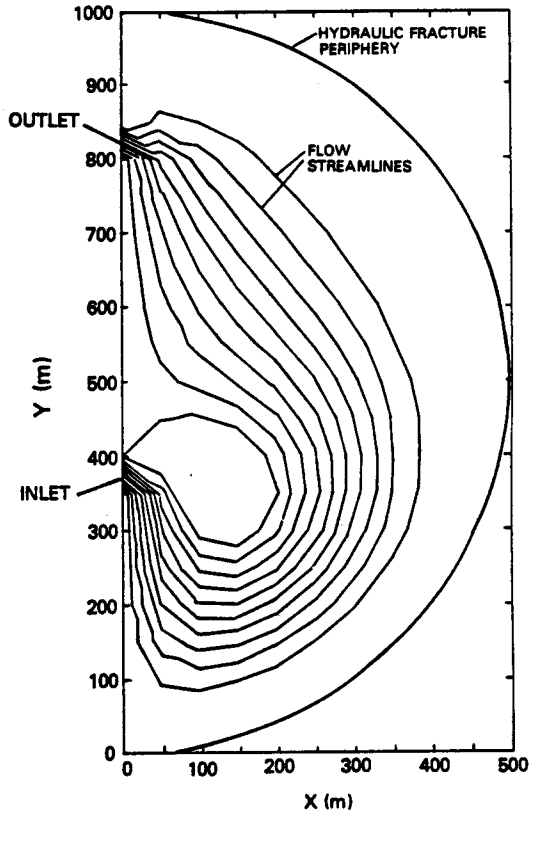

Fig. 32.
Flow streamlines with apprecible buoyancy contribution.

much of the area potentially available. In fact, only 40% of the total area is used effectively for heat transfer. In the second figure, the impedance is low enough that buoyancy is important. The cold entering fluid first flows downward due to its greater density, then eventually turns and flows to the outlet. In so doing, almost 90% of the total fracture area, more than twice that of the first case, is effective in heat transfer.

We propose the testing of these new modes of heat extraction in the old, Phase I reservoir. Since these new modes of heat transfer are ultimately aimed at developing techniques for increasing heat production from the Phase II reservoir, it might be argued that this testing should be delayed and conducted in the Phase II reservoir. However, after examining schedules and the currently depleted state of the Phase I reservoir, we believe that these new heat-extraction modes can most efficiently be demonstrated in the Phase I Reservoir because:

- o The Phase II reservoir schedule is very tight and precludes testing of new heat-transfer modes, even in the interim system, until 1983 or 1984.
- o The Phase II reservoir, even the interim system, is likely to be quite large and hot -- evaluation of new heat-extraction modes by means of thermal drawdown could take years.
- o In contrast, the Phase I reservoir is smaller and already thermally depleted. Beneficial effects of augmented heat transfer could be observed in several months.
- o The Phase I reservoir is available now, and depths and temperatures are much easier to work with. Use of the Phase I reservoir would not impact the Phase II schedule.

For these reasons we have designed new tests to be conducted in the Phase I reservoir. These tests are designated as Run Segments 6 and 7, to evaluate the cyclic and high-buoyancy modes of heat production, respectively. Test procedures are described below.

Run Segment 6 - Cyclic-Heat Production. Because of pumping and electrical-power restrictions, cyclic-heat production will be limited to an injection flow rate of 0.025 m^3/s (400 gpm). Previous testing, during SUE, was conducted at 0.044 m^3/s (700 gpm), and we are unsure of the results to be expected at the reduced flow rate. Consequently, a preliminary test, just one cycle, is necessary simply to check the hydraulic aspects at reduced flow

rate. Should these prove satisfactory, then a 6-month test consisting of 60 cycles would be employed to evaluate heat-transfer characteristics. (Should the hydraulic aspects be unsatisfactory, Run Segment 7, described next, would then be conducted.) Each cycle would consist of 1 day of injection with the existing pumps at the Fenton Hill site, followed by 2 days of venting. Injection would be into the normal injection well, EE-1, and venting would be from the normal production well, GT-2B. The existing data acquisition and control system would be used as well as the existing water-to-air heat exchangers. Wellhead pressures, flow rates, temperatures, and heat production rates would be continuously measured. Prior to Run Segment 6 a 10- to 15-day pumping period would be required to recharge the reservoir with about 7500 m^3 (2 000 000 gal) of water. This initial recharge would satisfy most of the reservoir water losses and thus would considerably simplify evaluation of the new mode of heat extraction that follows.

Run Segment 7 - High-Buoyancy Heat Production. As discussed earlier, high buoyancy requires low flow impedance, less than or equal to about 0.3 GPa s/m^3 (2.7 psi/gpm). To accomplish this, the impedance presently concentrated near the reservoir outlet should first be diminished by propping the fracture outlet. If completely successful, as much as 0.55 GPa s/m^3 (5 psi/gpm) of the present value of 1.1 GPa s/m^3 (10 psi/gpm) could be eliminated by such means. The residual main-fracture impedance would then be decreased by operating at high back pressure, that is, by operating at pressures high enough to inflate the fractures. A preliminary, 3-day experiment would be required to determine if the final impedance during high back-pressure conditions would be low enough to proceed with a long-term heat-extraction test. If this impedance was not low enough, no further testing would be conducted; but if it was satisfactorily low, a 3-month production test would ensue. As described above for Run Segment 6, the existing data acquisition, control and surface equipment would be used.

B. Improved Microseismic Mapping

Of paramount importance in the SUE was the use of the two-station method of locating events (see Figs. 33 and 34). It provided a more accurate map of the event locations than the previous single-station method. However, it still requires both the determination at one station of the absolute direction of the incoming signal from an event and the distance to the event (the hodogram-SP delay method). Each such location requires a considerable effort

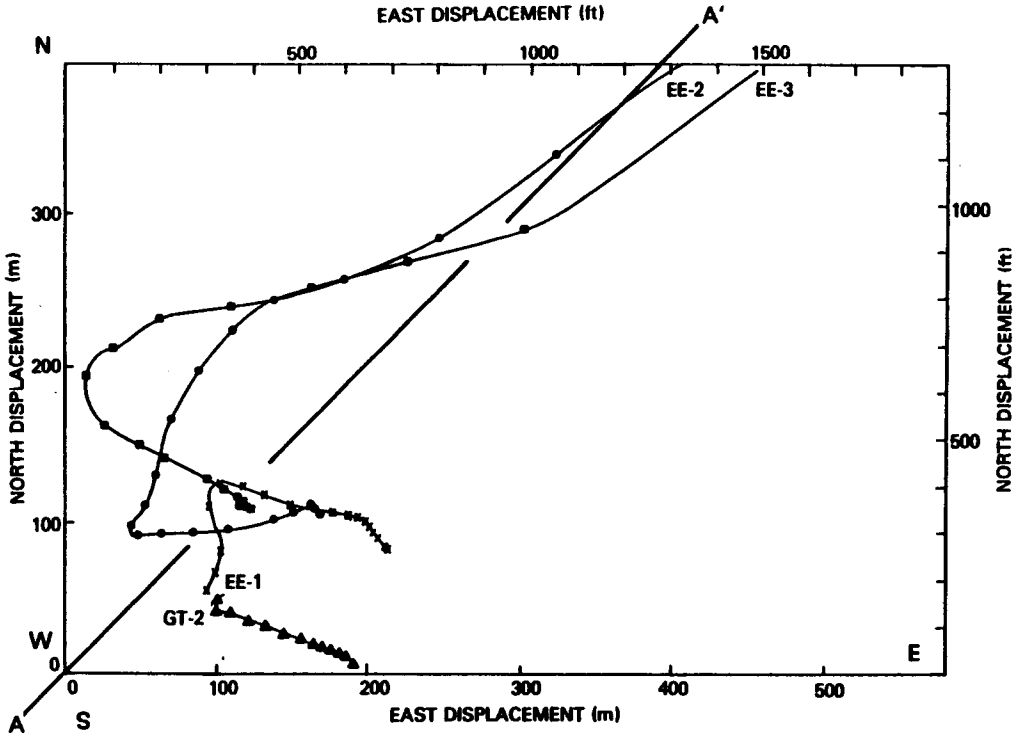

Fig. 33.
Plan view of the Fenton Hill wellbores.

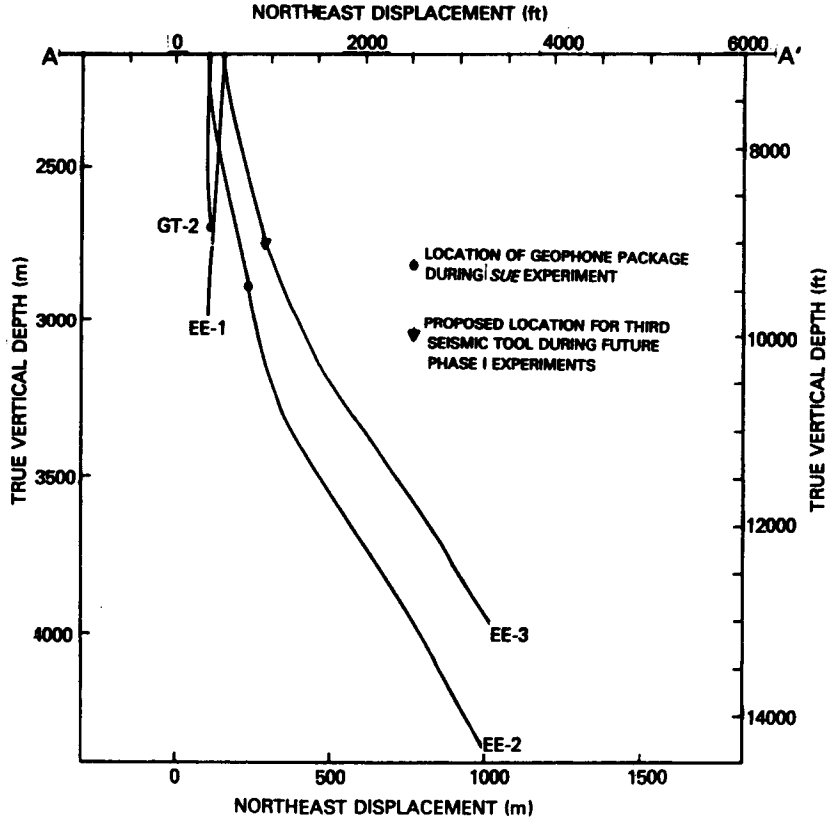

Fig. 34.
Elevation view of the Fenton Hill wellbores showing geophone package locations during SUE experiment and proposed location for additional seismic tool.

and would not be easily adapted to real-time analysis. The introduction of a third station (Fig. 34), however, would allow the use of the standard P-wave onset method for which sophisticated microprocessor equipment has been developed with the capability of such real-time analysis. Such a method would allow highly accurate mapping of essentially all of the events generated (over 10 000 in the SUE experiment). This degree of detail might reveal some of the finer structure such as groups of vertical joints and associated nonvertical connecting fractures.

C. Elucidation of Secondary Flow Paths

Geochemical evidence suggests that the large, hot, secondary flow paths could perhaps be exploited by increasing the injection pressure and lowering the production pressure. Increasing the injection pressure is relatively easy to accomplish, and decreasing the pressure in the production well could be accomplished by placing a downhole pump in GT-2B. This would prevent flashing of the fluid while simultaneously lowering the downhole pressure on the reservoir. Such an experiment could be used to establish the flow-rate limitations in the secondary flow paths and could eventually provide a time constant for the secondary flow portion of the reservoir.

Simultaneous pressurization and heat extraction by methods such as huff-puff may hold the key to opening the secondary flow paths to circulation and heat extraction. Evidence from the tracer studies indicates the profound changes that occur after pressurization and the regular changes in reservoir volume that accompany heat extraction. Pressure cycling the reservoir while extracting heat could dramatically accelerate the growth of the reservoir system.

REFERENCES

1. H. D. Murphy, R. G. Lawton, J. W. Tester, R. M. Potter, D. W. Brown, and R. L. Aamodt, "Preliminary Assessment of a Geothermal Energy Reservoir Formed by Hydraulic Fracturing," Soc. Petr. Eng. J. 17, 317-326 (1977).

2. J. W. Tester and J. N. Albright (eds.), "Hot Dry Rock Energy Extraction Field Test: 75 Days of Operation of a Prototype Reservoir at Fenton Hill," Los Alamos Scientific Laboratory report LA-7771-MS (April 1979).

3. H. D. Murphy and J. W. Tester, "Heat Production from a Geothermal Reservoir Formed by Hydraulic Fracturing--Comparison of Field and Theoretical Results," paper SPE 8265 presented at 54th Annual Mtg. of Soc. Petr. Engrs. of AIME, Las Vegas, Nevada, September 23-26, 1979.

4. D. W. Brown (ed.), "Results of Expt. 186, The High Back-Pressure Flow Experiment," Los Alamos National Laboratory report LA-8941-HDR (to be published).

5. H. D. Murphy (ed.), "Preliminary Evaluation of the Second Hot Dry Rock Geothermal Energy Reservoir: Results of Phase 1, Run Segment 4," Los Alamos Scientific Laboratory report LA-8354-MS (May 1980).

6. L. Aamodt and G. Zyvoloski, "Report on Phase 1, Segment 5, Stage 1 (Start Up of Experiment 217)," Los Alamos Scientific Laboratory G-5 internal report Tech. Memo #5 (April 21, 1980).

7. G. Zyvoloski (ed.), "Evaluation of the Second Hot Dry Rock Geothermal Energy Reservoir: Result of Phase I, Run Segment 5," Los Alamos National Laboratory report LA-8940-HDR (August 1981).

8. H. D. Murphy (ed.), "Relaxation of Geothermal Stresses Induced by Heat Production," Los Alamos National Laboratory report LA-8954-MS (August 1981).

9. A. W. Laughlin and A. C. Eddy, "Petrography and Geochemistry of Precambrian Rocks from GT-2 and EE-1," Los Alamos Scientific Laboratory informal report LA-6930-MS, 50 p. (August 1977).

10. A. W. Laughlin, "The Geothermal System of the Jemez Mountains, New Mexico and Its Exploration," in L. Rybach and L. J. P. Muffler (eds.), Geothermal Systems: Principals and Case Histories, John Wiley & Sons, Ltd., 295-320 (1981).

11. R. Laney, A. W. Laughlin, and M. J. Aldrich, "Geology and Geochemistry of Samples from Los Alamos National Laboratory HDR Well EE-2, Fenton Hill, New Mexico," Los Alamos National Laboratory report LA-8923-MS (July 1981).

12. A. W. Laughlin, A. C. Eddy, R. Laney, and M. J. Aldrich, "Geology of the Fenton Hill, New Mexico Hot Dry Rock Site," Los Alamos National Laboratory report (to be published).

13. D. G. Brookins, R. B. Forbes, D. L. Turner, A. W. Laughlin, and C. W. Naeser, "Rb-Sr, K-Ar and Fission-Track Geochronological Studies of Samples from LASL Drill Holes GT-1, GT-2, and EE-2," Los Alamos Scientific Laboratory report LA-6829-MS, 27 p. (June 1977).

14. R. D. McFarland and H. D. Murphy, "Extracting Energy from Hydraulically Fractured Geothermal Reservoir," in Proc. 11th Intersociety Energy Conversion Engineering Conference, State Line, Nevada, September 12-17, 1976.

15. F. H. Harlow and W. E. Pracht, "A Theoretical Study of Geothermal Energy Extraction," J. Geophys. Res. 77, 7038-7048 (1972).

16. H. D. Murphy, J. W. Tester, C. O. Grigsby, and R. M. Potter, "Energy Extraction from Fractured Geothermal Reservoirs in Low Permeability Crystalline Rock," J. Geophys. Res. (July 1981).

17. G. Zyvoloski, "Bottom-Hole Temperatures and pressures for Experiment 217," Los Alamos Scientific Laboratory G-5 internal report Tech. Memo #11 (November 7, 1980).

18. H. D. Murphy, "Thermal Stress Cracking and the Enhancement of Heat Extraction from Fractured Geothermal Reservoirs," Geothermal Energy 7, 22-29 (1979).

19. H. N. Fisher and J. W. Tester, "The Pressure Transient Testing of a Man-Made Fractured Geothermal Reservoir: An Examination of Fracture Versus Matrix Dominated Flow Effect," Los Alamos Scientific Laboratory report LA-8535-MS (September 1980).

20. J. W. Tester, R. M. Potter, and R. L. Bivins, "Interwell Tracer Analysis of a Hydraulically Fractured Granitic Geothermal Reservoir," paper SPE 8270 presented at 54th Annual Mtg. of Soc. Petr. Engrs. of AIME, Las Vegas, NV, September 23-26, 1979.

21. C. O. Grigsby, J. W. Tester, P. E. Trujillo, D. A. Counce, J. Abbott, C. E. Holley, and L. A. Blatz, "Rock-Water Interactions in Hot Dry Rock Geothermal Systems: Field Investigations of In Situ Geochemical Behavior," submitted to J. of Volcanology and Geothermal Research, 1981.

☆U.S. GOVERNMENT PRINTING OFFICE: 1981-0-576-020/160